Geochimica et Cosmochimica Acta 341 (2023) 75–89

Contents lists available at ScienceDirect

Geochimica et Cosmochimica Acta

journal homepage: www.elsevier.com/locate/gca

Mo isotopes archive oceanic sediments in post-orogenic lithospheric mantle

Feng Huang [a,*], Jie Li [b], Jifeng Xu [a], Jianlin Chen [b], Baodi Wang [c], Pan Hu [d], Rong Xu [e], Yunchuan Zeng [a], Le Zhang [b], Ting Zhou [e]

[a] State Key Laboratory of Geological Processes and Mineral Resources, and School of Earth Science and Resources, China University of Geosciences, Beijing 100083, China
[b] State Key Laboratory of Isotope Geochemistry, Guangzhou Institute of Geochemistry, Chinese Academy of Sciences, Guangzhou 510640, China
[c] China Aero Geophysical Survey and Remote Sensing Center for Natural Resources, Beijing 100083, China
[d] State Key Laboratory of Geological Processes and Mineral Resources, China University of Geosciences, Wuhan 430074, China
[e] State Key Laboratory of Ore Deposit Geochemistry, Institute of Geochemistry, Chinese Academy of Sciences, Guiyang 550081, China

ARTICLE INFO

Article history:
Received 18 May 2022
Accepted 22 November 2022
Available online 23 November 2022
Associate editor: Julie Prytulak

Keywords:
Mo isotopes
Ultrapotassic rocks
Oceanic sediments
Lithospheric mantle
Tethyan realm

ABSTRACT

The super-chondritic Mo isotopic composition of the continental crust has been attributed to contributions from subducted oceanic slabs and/or sediments, which introduce isotopically light Mo to the mantle. It has been hypothesized that dehydrated oceanic slabs subduct into the deep mantle and contribute to the genesis of ocean island basalts (OIBs). However, OIBs have similar average $\delta^{98/95}$Mo values (−0.22‰± 0.04‰; 2SE; n = 87) to the depleted mantle. Subducted oceanic sediments may create a light-$\delta^{98/95}$Mo reservoir in the subcontinental lithospheric mantle, but this has not been investigated in detail. Understanding the Mo isotopic systematics of the continental crust and mantle requires an understanding of the Mo isotopic composition of lithospheric mantle-derived volcanic rocks. The lithosphere in the Tibetan region has experienced multiple stages of oceanic subduction and is thus ideal for studying magmas derived from sediment-modified lithospheric mantle. Mafic ultrapotassic volcanic rocks (UPVRs) from the Sailipu area on the southern Tibetan Plateau have high Mg# values (67.1–72.5) and enriched Sr–Nd isotopic compositions and are primitive magmas derived from the lithospheric mantle. These rocks have higher Ce/Mo ratios (225–422) and lighter $\delta^{98/95}$Mo values (−0.45‰ to −0.13‰) than the depleted mantle, mid-ocean ridge basalts (MORBs), and OIBs, as well as high $\varepsilon_{Hf}(t)$ values at given $\varepsilon_{Nd}(t)$ values compared with the terrestrial array ($\Delta\varepsilon_{Hf}$ = 4.59–5.73). The involvement of Ca-poor pelagic sediments rather than the lower continental crust and hydrated oceanic slab best accounts for the high Ce/Mo ratios and light $\delta^{98/95}$Mo values of the studied rocks. The Sailipu UPVRs also have higher Nb/Ta (18.9–20.8) and Th/La (2.6–3.4) ratios than arc-related igneous rocks and MORBs, suggesting that their source was phlogopite-bearing lithospheric mantle with a metasomatic vein component (rutile + monazite ± lawsonite). We propose a two-stage geodynamic process to explain the formation of the Sailipu UPVRs: (1) a metasomatic vein component with high Th/La and Ce/Mo ratios formed in the lithospheric mantle during multiple stages of oceanic subduction; (2) high mantle temperatures related to convective thinning of the lithosphere resulted in melting of the vein component and the ambient mantle, which produced hybrid melts of various mantle domains during the post-orogenic stage. The Sailipu UPVRs have enriched Sr–Nd isotopic compositions and high Th/La and Ce/Mo ratios, similar to lamproites that are widespread in the Tethyan orogenic realm from the Mediterranean to the southern Tibetan Plateau. Given that UPVRs with light $\delta^{98/95}$Mo values have also been identified in the Western Alps, we propose that the isotopically light Mo component is widespread in Tethyan lithospheric mantle. This isotopically light Mo in the lithospheric mantle may be a complementary end-member to the isotopically heavier continental crust. The recycling of subducted oceanic sediments has a key role in the deep recycling of Mo.

* Corresponding author at: 29 Xueyuan Road, Haidian District, Beijing 100083, China.
E-mail address: fenghuang@cugb.edu.cn (F. Huang).

https://doi.org/10.1016/j.gca.2022.11.023
0016-7037/

1. Introduction

Molybdenum (Mo) is a redox-sensitive element, highly mobile on Earth's surface, and its isotopes are strongly fractionated by low-temperature processes (e.g., Willbold and Elliott, 2017). Molybdenum is generally a refractory and incompatible element in magmatic systems, and Mo^{4+} preferentially retains lighter Mo isotopes and is more compatible than Mo^{6+} (Leitzke et al., 2017). These geochemical properties lead to changes in the coordination and charge of Mo during various geological processes at high and low temperatures; therefore, Mo isotopes can be used to trace crust–mantle recycling. The bulk silicate Earth (BSE) has a $\delta^{98/95}$Mo value of −0.21‰ ± 0.06‰ ($\delta^{98/95}Mo = [(^{98}Mo/^{95}Mo)_{sample}/(^{98}Mo/^{95}Mo)_{standard} - 1] \times 1000$, where the subscript "standard" represents the National Institute of Standards and Technology [NIST] reference material 3134), based on studies of meteorites and komatiites (Burkhardt et al., 2014; Greber et al., 2015; Liang et al., 2017). The depleted mantle has an identical $\delta^{98/95}$Mo value (–0.21‰ ± 0.02‰; Bezard et al., 2016; Liang et al., 2017; McCoy-West et al., 2019) to the BSE, which is lighter than that of the continental crust ($\delta^{98/95}$Mo = 0.05–0.15‰; Chen et al., 2022a; Greber et al., 2014; Voegelin et al., 2014; Willbold and Elliott, 2017). It has been speculated that this difference in $\delta^{98/95}$Mo between the BSE and the continental crust is the result of subduction processes, and it may be due to the presence of isotopically lighter Mo reservoirs on Earth, such as the deep mantle (e.g., the transition zone, lower mantle, or at the core–mantle boundary; Liang et al., 2017; Willbold and Elliott, 2017).

Arc volcanic rocks have variable $\delta^{98/95}$Mo values from − 1.91‰ to 1.10‰ (mean = − 0.07‰ ± 0.04‰; 2SE; n = 227; Ahmad et al., 2021; Freymuth et al., 2015, 2016; Gaschnig et al., 2017; König et al., 2016; Li et al., 2021a, 2021b; Villalobos-Orchard et al., 2020; Voegelin et al., 2014; Wille et al., 2018; Zhang et al., 2020), and most have heavier $\delta^{98/95}$Mo values (>0‰) than the depleted mantle (−0.21‰ ± 0.02‰; Bezard et al., 2016; Liang et al., 2017; Willbold and Elliott, 2017). The wide range of Mo isotopic compositions in arc igneous rocks has been attributed to isotopically heavy Mo that is partitioned into slab-derived fluids, whereas isotopically light Mo is retained in the residual subducting oceanic crust and/or sediments (Aarons et al., 2021; Freymuth et al., 2015; Gaschnig et al., 2017; Villalobos-Orchard et al., 2020; Willbold and Elliott, 2017). As such, the subducted slab and overlying sediments with light $\delta^{98/95}$Mo values best explain the Mo isotope balance between the BSE and the continental crust. The incorporation of isotopically light Mo from devolatilized subducted oceanic crust into the deep mantle has been investigated in several studies (Gaschnig et al., 2021a, 2021b; Liang et al., 2017; Ma et al., 2022; Yang et al., 2015). However, an alternative potential reservoir (i.e., the lithospheric mantle) has been largely neglected, and this reservoir may store isotopically light $\delta^{98/95}$Mo derived from sediments introduced during protracted oceanic subduction.

The Tibetan–Himalaya Orogen is the largest, present-day, continental collisional belt on Earth and has experienced multiple stages of oceanic subduction (including in the Paleo-, meso-, and NeoTethys oceans) since the Paleozoic (Kapp and DeCelles, 2019; Zhu et al., 2013). Post-orogenic ultrapotassic volcanic rocks (UPVRs) are widely developed on the southern Tibetan Plateau and are characterized by high Mg# values ($100 \times Mg^{2+}/[Mg^{2+}+Fe^{2+}] > 65$), high MgO (>6 wt%) and compatible trace element (e.g., Cr and Ni) contents, and enriched Sr–Nd isotopic compositions, and they thus represent primitive magmas derived from the lithospheric mantle (Guo and Wilson, 2019; Guo et al., 2015; Huang et al., 2015; Miller et al., 1999; Williams et al., 2004). These post-orogenic UPVRs occur from the Himalayas through to the Alps over a distance of ~10,000 km (Casalini et al., 2021; Tommasini et al., 2011) and are ideal for studying the Mo isotopic systematics of magmas derived from subcontinental lithospheric mantle that has been modified by subducted materials. This study reports Mo isotope data for UPVRs from the southern Tibetan Plateau, along with geochemical and Sr–Nd–Hf isotope data. Our results show that the UPVRs have high Ce/Mo ratios and isotopically light Mo, which are distinct from mid-ocean ridge basalts (MORBs) and ocean island basalts (OIBs). The correlations between $\delta^{98/95}$Mo values and some geochemical parameters (e.g., Th/La and Nb/Ta ratios) suggest that recycled pelagic sediment in the lithospheric mantle is the most probable source of the isotopically light Mo in the UPVRs. We propose that this light-$\delta^{98/95}$Mo lithospheric component may potentially balance the Mo isotopic systematics of the BSE and continental crust.

2. Geological setting and samples

The Tibetan–Himalaya orogenic system comprises several micro-continents that drifted away from Gondwanaland after the Paleozoic before their final amalgamation during the Cenozoic India–Asia continental collision (e.g., Yin and Harrison, 2000). The Tibetan Plateau comprises the Songpan–Ganzi complex, Qiangtang Terrane, Lhasa Terrane, and Himalaya (from north to south). The Lhasa Terrane is bounded by the Bangong–Nujiang suture (BNS) and Indus–Yarlung Zangbo suture (IYZS) to the north and south, respectively (Fig. 1). After the onset of the India–Asia continental collision, three types of Cenozoic magmatism occurred throughout the Lhasa Terrane: (1) the 65–40 Ma calc-alkaline Gangdese batholith and Linzizong volcanic rocks (Fig. 1; e.g., Lee et al., 2009; Liu et al., 2022a; Zhang et al., 2022), which were related to NeoTethyan subduction; (2) 30–10 Ma adakitic igneous rocks that represent melts of thickened lower continental crust (e.g., Chen et al., 2011; Chung et al., 2003); and (3) 26–8 Ma ultrapotassic and potassic volcanic rocks (Fig. 1) derived from the lithospheric mantle (e.g., Guo and Wilson, 2019; Guo et al., 2015; Huang et al., 2015; Miller et al., 1999; Zhao et al., 2009). The ultrapotassic and potassic volcanic rocks are exposed as small-volume lava flows and dikes close to a series of N—S—trending rifts (Fig. 1; e.g., Guo et al., 2013, 2015; Huang et al., 2015; Williams et al., 2004).

The Sailipu UPVRs formed at 18.5–17.0 Ma and are located in the Sailipu Basin, western Lhasa Terrane, southern Tibetan Plateau (Guo et al., 2015; Wang et al., 2008; Zhao et al., 2009). These rocks form discontinuous, small-volume lava flows that are a few hundred meters to a few kilometers in length and 1–100 m thick. The Sailipu UPVRs overlie Paleozoic–Mesozoic strata and the Linzizong volcanic rocks (Wang et al., 2014). Most samples are porphyritic with phenocrysts of phlogopite, clinopyroxene, and subordinate olivine (Fig. S1) set in a groundmass of olivine, phlogopite, clinopyroxene, sanidine, Fe–Ti oxides, and glass.

3. Analytical methods

Twenty-three whole-rock samples with unweathered surfaces were cut into small slices and cleaned ultrasonically in distilled water. The dried whole-rock samples were crushed to < 1 mm and then powdered in an agate mortar. The final powder (<200 mesh) was used for geochemical analysis. Loss-on-ignition (LOI) values were determined by heating ~0.5 g of sample powder in a porcelain crucible for 1.5 h at 1000 °C. Whole-rock major element data were obtained by X-ray fluorescence (XRF) spectrometry on fused glass discs using a PANalytical AXIOS Minerals instrument at the Rock–Mineral Preparation and Analysis Laboratory, Institute of Geology and Geophysics, Chinese Academy of Sciences (IGGCAS),

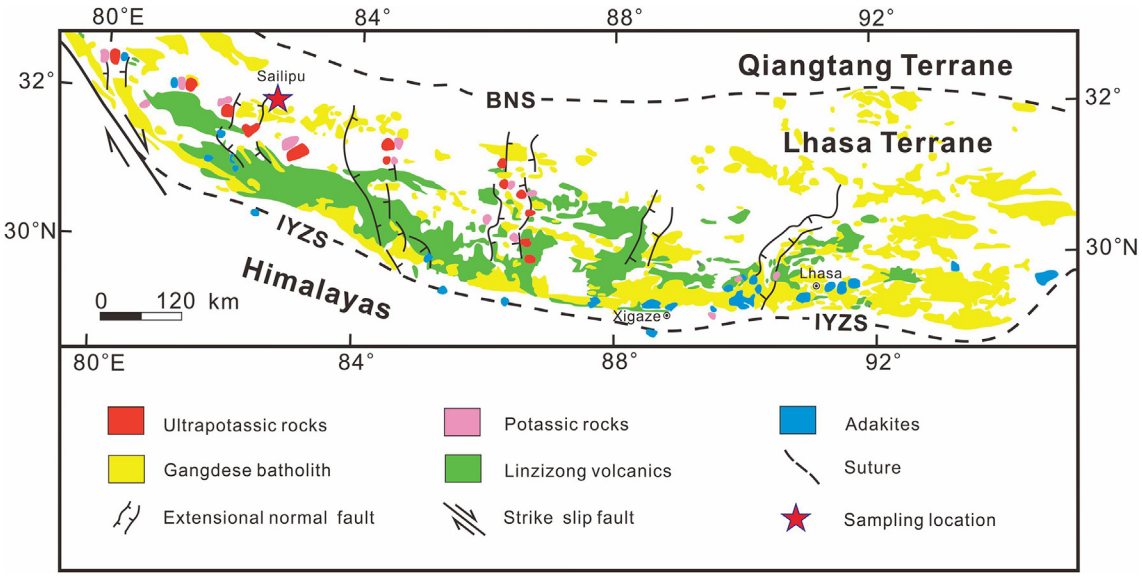

Fig. 1. Sketch map showing the distribution of Cenozoic magmatic rocks in southern Tibetan Plateau (modified from Guo et al., 2015) Sampling locations in this study are also shown. Abbreviation: BNS = Bangong-Nujiang Suture; IYZS = Indus-Yarlung Zabong Suture.

Beijing, China. The analytical uncertainty of the major element data was < ± 3%. Sample aliquots (~50 mg) were digested in HNO_3 + HF in high-pressure Teflon bombs for 48 h to ensure complete dissolution. Trace element contents were then measured using a Thermo iCAP Q inductively coupled plasma mass spectrometer (ICP–MS) at the Guangzhou Institute of Geochemistry, Chinese Academy of Sciences (GIGCAS), Guangzhou, China. The analytical uncertainty of the trace element data was < ± 10%. Details of the analytical procedures have been described by Huang et al. (2021).

Chemical separation of whole-rock Sr-Nd-Hf isotopes were conducted at the Guilin University of Technology, Guilin, China (GUT). Strontium–Nd and Hf isotope ratios were determined at the GUT and Institute of Geochemistry, Chinese Academy of Sciences, respectively. Sample powders (~50 mg) were dissolved in distilled HNO_3 + HF in screw-top PFA beakers at 120 °C for at least 7 d. Strontium was separated using a Sr-specific resin. Rare earth elements (REEs) were separated using ion exchange columns, and Nd was isolated on HDEHP-coated Kef columns. Determination of Sr–Nd isotope ratios employed a Neptune Plus multi-collector (MC)–ICP–MS using the procedures described by Huang et al. (2019). Repeated measurement of NBS SRM 987 yielded $^{87}Sr/^{86}Sr$ = 0.710250 ± 6 (2σ; n = 7) and of JNdi-1 yielded $^{143}Nd/^{144}Nd$ = 0.5 12093 ± 5 (2σ; n = 7). BHVO-2 was analyzed to monitor the data accuracy and yielded $^{87}Sr/^{86}Sr$ = 0.703512 ± 6 (2σ; n = 4) and $^{143}Nd/^{144}Nd$ = 0.512988 ± 5 (2σ; n = 4), consistent with the recommend values for this standard (GeoReM; https://georem.mpch-mainz.gwdg.de/).

For Hf isotope analysis, sample powders were digested in a 1:3 mixture of HNO_3 + HF in Savillex beakers at 120 °C for 5 d. The solutions were then evaporated and 6 N HCl was added to the residue, which was then heated for 24 h. These steps were repeated two or three times until the solution was completely clear. Hafnium was separated using a modified ion exchange procedure using a single column and Ln-specific resin. Hafnium isotope ratios were measured using a Neptune Plus MC–ICP–MS. The $^{176}Hf/^{177}Hf$ ratios were normalized to the JMC-475 Hf standard ($^{176}Hf/^{177}Hf$ = 0.282160). BCR-2 yielded $^{176}Hf/^{177}Hf$ = 0.282864 ± 8 (2σ; n = 4).

Chemical separation of Mo was conducted at the Guizhou Tongwei Analytical Technology Company Limited, Guizhou, China, using the analytical protocols described by Li et al. (2014). Approximately 0.1–0.2 g of sample powder was spiked with a double isotope tracer (^{97}Mo–^{100}Mo). The spiked samples were digested in HF + HNO_3 in beakers at 150 °C for 3 d. The Mo separation was undertaken using *N*-benzoyl-*N*-phenylhydroxylamine (BPHA) resin. Molybdenum isotope data were obtained using a Neptune Plus MC–ICP–MS at the GIGCAS, and the double-spike method was used to correct for instrumental mass bias. The Mo isotopic composition is expressed as $\delta^{98/95}Mo$ relative to the NIST SRM 3134 standard. The external reproducibility of the $\delta^{98/95}Mo$ values for the NIST SRM 3134 is ± 0.06‰ (2SD; n = 19). The total procedural blanks for Mo were 0.30 ± 0.15 ng (2SD; n = 4). IAPSO seawater and the rock standards W-2a and AGV-2 were also analyzed and yielded $\delta^{98/95}Mo$ values of 2.06‰± 0.03‰, −0.04‰ ± 0.06‰, and −0.14‰ ± 0.03‰, respectively (Table 1). The $\delta^{98/95}Mo$ values of these standards are consistent with those from previous studies (Chen et al., 2019; Willbold et al., 2016; Zhao et al., 2016). Molybdenum contents were determined using the isotope dilution method. IAPSO seawater and the rock standards W-2a and AGV-2 yielded Mo contents of 10.4 ppb, 0.45 ppm, and 1.99 ppm, respectively. Replicate dissolution and analysis of samples SLP-11 and SLP-18 yielded consistent $\delta^{98/95}Mo$ values (Table 1).

4. Results

4.1. Major and trace elements

The Sailipu UPVRs plot in the basaltic trachyandesite and trachyandesite fields in a total alkalis ($Na_2O + K_2O$)–SiO_2 plot, consistent with previous studies of such rocks from the Sailipu area and other mafic ultrapotassic rocks on the southern Tibetan Plateau (Fig. 2a; Gao et al., 2007; Guo and Wilson, 2019; Guo et al., 2013, 2015; Huang et al., 2015; Miller et al., 1999; Tian et al., 2020). The studied rocks have relatively primitive compositions with high Mg# values (67.1–72.5; assuming all Fe is Fe^{2+}) and high MgO (6.70–8.15 wt. %), Cr (299–590 ppm), and Ni (195–369 ppm) contents (Table S1). The samples have high K_2O contents and K_2O/Na_2O ratios of 6.34–7.99 wt. % and 3.26–4.78, respectively (Fig. 2b). The Sailipu UPVRs are orogenic lamproites, similar to those in the Mediterranean region (Figs. 2c and S2), based on the classification scheme of Foley et al. (1987).

Table 1
Mo isotope and selected element and Sr-Nd-Hf isotope data for the Sailipu ultrapotassic rocks in southern Tibetan Plateau.

Sample	Mo (ppm)	$\delta^{98/95}$Mo (‰)	2SE	SiO_2 (wt. %)	Mg#[b]	Ce (ppm)	Ce/Mo	Cu/Mo	Th/La	Nb/Ta	$^{87}Sr/^{86}Sr_i$	$^{143}Nd/^{144}Nd_i$	$\varepsilon_{Nd}(t)$	$\varepsilon_{Hf}(t)$	$\Delta\varepsilon_{Hf}(t)$[c]
SLP-03	0.64	−0.24	0.06	53.68	69.4	229.1	357	98	3.3	19.7	0.726655	0.511850	−14.93	−16.73	5.20
SLP-05	0.89	−0.42	0.04	54.68	71.4	220.1	248	55	3.1	19.9	0.726630	0.511838	−15.15	−17.35	4.93
SLP-07	0.88	−0.39	0.05	52.86	68.5	217.1	248	63	2.6	19.7	0.725012	0.511862	−14.69	−16.23	5.34
SLP-09	0.76	−0.20	0.05	54.31	68.3	229.7	303	95	3.3	19.3	0.726447	0.511842	−15.08	−16.47	5.70
SLP-10–2	0.69	−0.30	0.05	55.79	71.8	236.1	343	42	2.8	19.5	0.726835	0.511810	−15.70	−18.52	4.59
SLP-11	0.92	−0.45	0.05	54.97	70.5	228.7	249	109	3.4	19.4	0.726645	0.511848	−14.97		
SLP-11-R[a]	0.88	−0.43	0.06												
SLP-12	0.62	−0.31	0.05	54.45	72.5	260.7	422	59	3.3	20.4	0.727457	0.511815	−15.60	−18.12	4.85
SLP-14	1.11	−0.28	0.04	55.66	71.2	280.4	252	41	3.2	19.4	0.726791	0.511810	−15.70	−18.19	4.94
SLP-15–2	0.54	−0.13	0.07	53.65	68.8	181.2	333	132	3.0	18.9	0.726687	0.511839	−15.14	−16.92	5.34
SLP-16	0.97	−0.44	0.04	54.52	70.7	218.7	225	55	3.1	19.8	0.726589	0.511851	−14.89	−17.06	4.82
SLP-18	0.88	−0.26	0.05	54.80	68.9	214.0	244	71	2.7	20.0	0.725485	0.511860	−14.72	−15.87	5.73
SLP-18-R[a]	0.87	−0.22	0.07												

Standards	Mo (ppm)	2SD	$\delta^{98/95}$Mo	2SD	n	References
AGV-2	1.99	0.02	−0.14	0.03	4	This study
AGV-2	1.96	0.05	−0.15	0.01	3	Willbold et al. (2016)
W-2a	0.45	0.05	−0.04	0.06	5	This study
W-2a	0.41	0.03	−0.03	0.04	13	Chen et al. (2019)
IAPSO seawater	0.01	0.001	2.06	0.03	4	This study
IAPSO seawater	0.01	0.001	2.02	0.06	20	Zhao et al. (2016)
Blank	0.00030	0.00015			4	This study

[a] R: duplicate sample.
[b] Mg# = $Mg^{2+}/(Mg^{2+} + Fe^{2+}) \times 100$, assuming total Fe is Fe^{2+}.
[c] $\Delta\varepsilon_{Hf}(t) = \varepsilon_{Hf}(t) - 1.55 \times \varepsilon_{Nd}(t) - 1.21$] (Vervoort et al., 2011).

The Sailipu UPVRs are enriched in light rare earth elements (REEs) and have relatively flat heavy REE patterns, with small negative Eu anomalies (Fig. 3). Primitive mantle-normalized multi-element patterns (Fig. 3) exhibit significant enrichments in large-ion lithophile elements (e.g., Rb and U) and negative Nb, Ta, and Ti anomalies, despite their high contents (Table S1). These trace element patterns are similar to those of lamproites from the Mediterranean region (Casalini et al., 2021, and references therein) that formed during the Alpine–Himalayan orogeny.

4.2. Strontium–Nd–Hf isotopes

The initial Sr, Nd, and Hf isotope ratios were corrected to 18 Ma (Guo et al., 2015; Wang et al., 2008). The Sailipu UPVRs have radiogenic $^{87}Sr/^{86}Sr_i$ (0.725012–0.727457) and unradiogenic $^{143}Nd/^{144}Nd_i$ (0.511810–0.511869) values, corresponding to $\varepsilon_{Nd}(t)$ values of −15.70 to −14.56 (Fig. 4a; Table S2). In agreement with previous studies (Cheng and Guo, 2017; Guo and Wilson, 2019; Guo et al., 2015; Tian et al., 2020; Wang et al., 2014; Zhao et al., 2009), the $^{87}Sr/^{86}Sr_i$ and $\varepsilon_{Nd}(t)$ values of the Sailipu UPVRs are much higher and lower, respectively, than those of lamproites from the Mediterranean region (Fig. S3; Casalini et al., 2021, and references therein). The Sailipu UPVRs have low $^{176}Hf/^{177}Hf_i$ ratios (0.282237–0.282312) and $\varepsilon_{Hf}(t)$ values (−18.52 to −15.87). They have high $\varepsilon_{Hf}(t)$ values at given $\varepsilon_{Nd}(t)$ values relative to the $\varepsilon_{Nd}(t)$–$\varepsilon_{Hf}(t)$ terrestrial array (Fig. 4b), with $\Delta\varepsilon_{Hf}(t)$ ($\varepsilon_{Hf}(t) - 1.55 \times \varepsilon_{Hf}(t) - 1.21$; Vervoort et al., 2011) of 4.59–5.73 (Table 1). The unradiogenic Nd signature of the Sailipu UPVRs likely reflects a contribution from zircon-free sediments (Bayon et al., 2009).

4.3. Molybdenum isotopes

The Sailipu UPVRs have Mo contents of 0.54–1.11 ppm, similar to those of MORB (0.07 –1.93 ppm; Bezard et al., 2016; Chen et al., 2022b). The Ce/Mo ratios of the Sailipu UPVRs are 225–422, much higher than those of MORB (~34; Gale et al., 2013) but similar to Mediterranean lamproites (Fig. 5a; Casalini, 2018; Casalini et al., 2019). This characteristic is notably different from other subduction-related igneous rocks (Freymuth et al., 2015; Gaschnig et al., 2017; König et al., 2016; Li et al., 2021a, 2021b; Villalobos-Orchard et al., 2020; Voegelin et al., 2014; Wille et al., 2018). There are no correlations between Mo contents and $\delta^{98/95}$Mo with indices of magmatic differentiation, such as Mg# values (Fig. S4). The samples have $\delta^{98/95}$Mo = −0.45‰ to −0.13‰ (Table 1), and the $\delta^{98/95}$Mo values exhibit negative and positive correlations with Mo contents and Ce/Mo ratios, respectively (Figs. 5c and e). These UPVRs have significantly lighter $\delta^{98/95}$Mo values than MORB and depleted mantle (Bezard et al., 2016; Chen et al., 2022b; Liang et al., 2017; Willbold and Elliott, 2017), similar to those of Mediterranean lamproites (Fig. 5c; Casalini, 2018), subduction-related igneous rocks (Ahmad et al., 2021; Freymuth et al., 2015, 2016; Gaschnig et al., 2017; König et al., 2016; Li et al., 2021a, 2021b; Villalobos-Orchard et al., 2020; Wille et al., 2018; Zhang et al., 2020), and MORB-type eclogites (Fig. 5e; Ahmad et al., 2021; Chen et al., 2019).

5. Discussion

5.1. Sailipu UPVRs: primitive Alpine–Himalayan orogenic lamproites

The Sailipu UPVRs have low CaO (<8 wt. %), Al_2O_3 (<13 wt. %), and Na_2O (<2 wt. %) contents, high K_2O (>6 wt. %) and MgO (>6 wt. %) contents, and high Mg# values (67.1–72.5) (Table S1), typical of lamproites as defined by Foley et al. (1987). Such UPVRs have been found in scattered outcrops of hypabyssal and volcanic rocks (i.e., Alpine lamproites) along the Tethyan orogenic belts (Tommasini et al., 2011). Geochemical data for UPVRs in the southern Tibetan Plateau and the Mediterranean region were screened

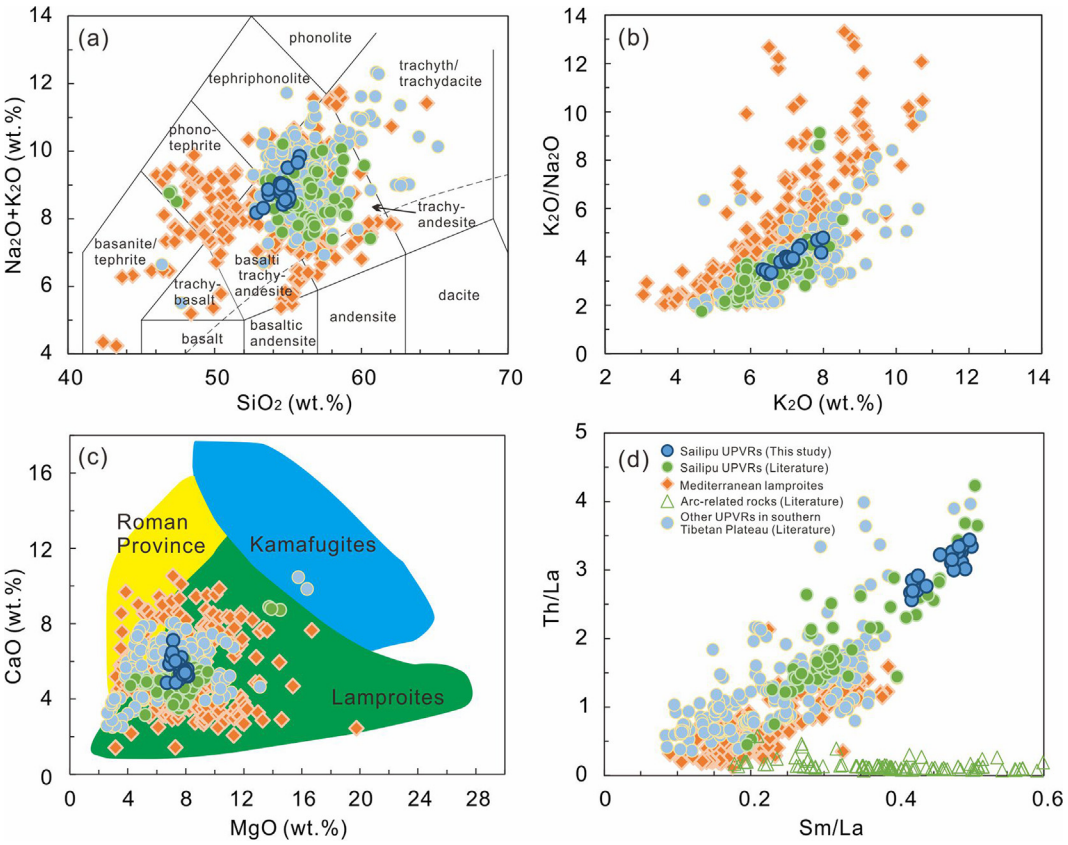

Fig. 2. Plots of (a) SiO_2 (wt. %) versus $Na_2O + K_2O$ (wt. %), (b) K_2O (wt. %) versus K_2O/Na_2O ratios, (c) MgO (wt. %) versus CaO (wt. %) and (d) Sm/La versus Th/La ratios for the southern Tibetan ultrapotassic rocks (UPVRs), Mediterranean lamproites and arc-related rocks. Data source: published Sailipu UPVRs (Cheng and Guo, 2017; Guo and Wilson, 2019; Guo et al., 2015; Tian et al., 2020; Wang et al., 2014; Zhao et al., 2009), other UPVRs in southern Tibetan Plateau (Gao et al., 2007; Guo and Wilson, 2019; Guo et al., 2013, 2015; Huang et al., 2015; Miller et al., 1999; Tian et al., 2020), Mediterranean lamproites (Casalini et al., 2021 and reference therein), arc-related rocks (Ahmad et al., 2021; Freymuth et al., 2016; Freymuth et al., 2015; Gaschnig et al., 2017; König et al., 2016; Li et al., 2021a; Li et al., 2021b; Villalobos-Orchard et al., 2020; Wille et al., 2018; Zhang et al., 2020).

to exclude rocks with MgO < 6 wt. % to minimize the effects of magmatic differentiation. The Sailipu UPVRs exhibit a positive correlation between K_2O contents and K_2O/Na_2O ratios, similar to published data for Alpine lamproites (Fig. 2b). In addition, they exhibit positive correlations between Sm/La and Th/La ratios and have the highest Th/La ratios (>2.5) reported to date for Alpine–Himalayan orogenic lamproites (Fig. 2d). This correlation is different to that exhibited by arc igneous rocks (i.e., a negative correlation with Th/La < 0.5; Fig. 2d; Casalini et al., 2021; Plank, 2005; Tommasini et al., 2011; Wang et al., 2021). Curved trends are observed on plots of Th/La–$^{87}Sr/^{86}Sr_i$ and Th/La–$^{143}Nd/^{144}Nd_i$, with the Sailipu and other high-MgO UPVRs from the southern Tibetan Plateau having more enriched isotopic compositions than those in the Mediterranean region (Fig. S3). This indicates that the UPVRs from the southern Tibetan Plateau contain a more enriched component than most Tethyan lamproites. In the subsequent sections, we discuss the geological processes that controlled the Mo contents and isotopic compositions of the studied rocks, and then identify the likely mechanisms that generated the Mo isotopic variations in the post-orogenic lithospheric mantle.

5.2. Effects of alteration, crustal contamination, and magmatic processes

5.2.1. Alteration and crustal contamination

Volcanic rocks are susceptible to low-temperature alteration (i.e., weathering). Given that fluids incorporate Mo and other mobile elements (Bali et al., 2012; Gaschnig et al., 2021b), weathering may result in Mo depletion and high Ce/Mo ratios, along with changes in other ratios between mobile (e.g., Rb and Ba) and immobile (e.g., Th) elements. Weathering-related Mo depletion would cause a negative correlation between Ce/Mo and Ba/Th ratios; however, the studied UPVRs do not exhibit such a trend (Fig. S5). In addition, the Sailipu UPVRs have low LOI (<3 wt. %) and chemical index of alteration (45–47) values, and the Mo contents and $\delta^{98/95}$Mo values do not vary systematically with LOI values (Table S1). This indicates that alteration did not affect the Mo isotope data.

Several studies have proposed that UPVRs are likely derived from the subcontinental lithospheric mantle (Gao et al., 2007; Huang et al., 2015; Williams et al., 2004) and are perhaps contaminated by crustal materials during magma ascent (Liu et al., 2014). The Mo contents of the UPVRs (0.54–1.11 ppm) are generally lower than those of the upper continental crust (1.1 ppm; Rudnick and Gao, 2014). The upper continental crust has isotopically heavier Mo ($\delta^{98/95}$Mo = 0.05–0.15‰; Chen et al., 2022a; Greaney et al., 2018; Voegelin et al., 2014) than the depleted mantle ($\delta^{98/95}$Mo = −0.21‰ ± 0.02‰; Bezard et al., 2016; Willbold and Elliott, 2017), and crustal contamination would increase both the Mo contents and $\delta^{98/95}$Mo values. However, the negative correlation between Mo contents and $\delta^{98/95}$Mo values (Fig. 5c) indicates that crustal contamination was negligible.

Other lines of evidence are also consistent with the inferred negligible crustal contamination: (1) the high Mg# values (mean = 70) and MgO contents (6.70–8.15 wt. %; Table S1); (2)

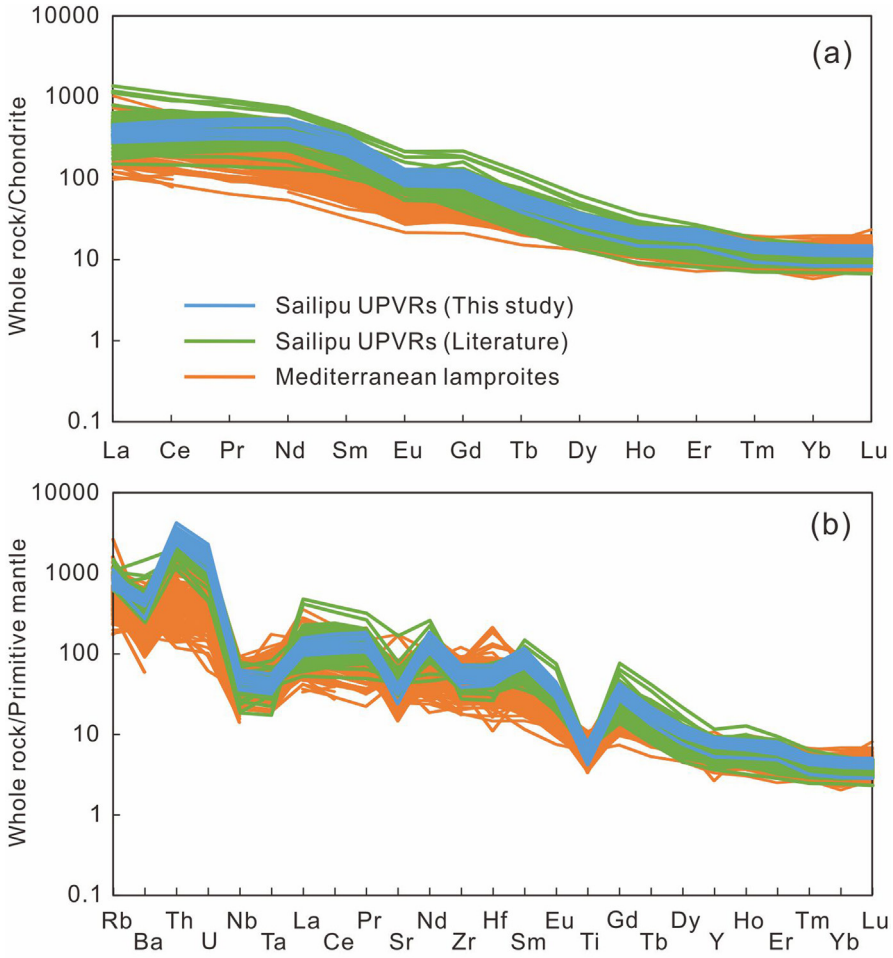

Fig. 3. Chondrite normalized REE and primitive mantle normalized (Sun and McDonough, 1989) incompatible trace element patterns of Sailipu UPVRs and Mediterranean lamproites. Data sources as in Fig. 2.

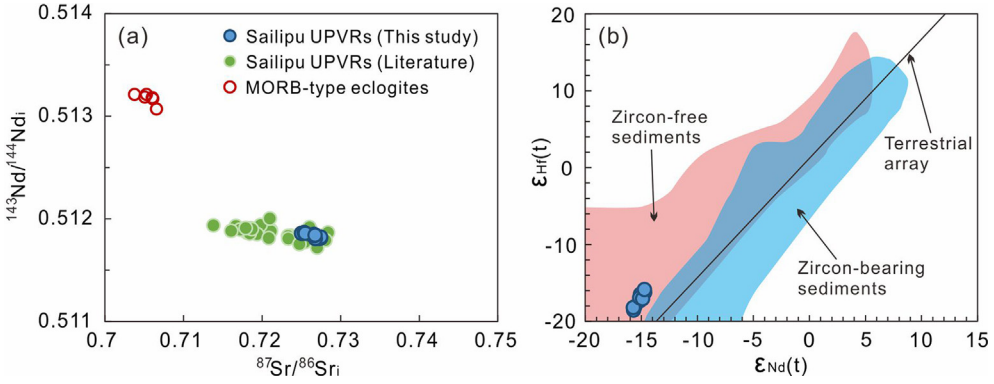

Fig. 4. Radiogenic Sr–Nd–Hf isotope composition of Sailipu UPVRs in southern Tibetan Plateau. Data sources: Sailipu UPVRs as in Fig. 2, MORB-type eclogites (Chen et al., 2019), Terrestrial array (Vervoort et al., 2011), zircon-free and zircon-bearing sedimentary rocks (Bayon et al., 2009).

incompatible trace element contents that are several times higher than that of the continental crust (Fig. 3); and (3) the mantle xenoliths entrained in the UPVRs (Cheng and Guo, 2017; Liu et al., 2011).

5.2.2. Fractional crystallization

As a result of cooling during magma ascent, fractional crystallization may cause changes in Mo contents and isotopic compositions. Previous studies have identified negligible Mo isotopic fractionation in H_2O-poor tholeiitic basalts to rhyolites from Hekla, southern Iceland, which have uniform MORB-like $\delta^{98/95}$Mo values (−0.15‰ ± 0.05‰; Yang et al., 2015). This is also consistent with data for another tholeiitic suite from the Kilauea Iki lava lake in Hawaii (Gaschnig et al., 2021a). Octahedrally coordinated Mo has a similar ionic radii to Ti, which leads to substantial incorporation of Mo into Fe–Ti oxides (Greaney et al., 2017). A study of cumulate rocks from the Windimurra layered intrusion identified small Mo isotopic variations in tholeiitic rocks (Nebel-Jacobsen et al.,

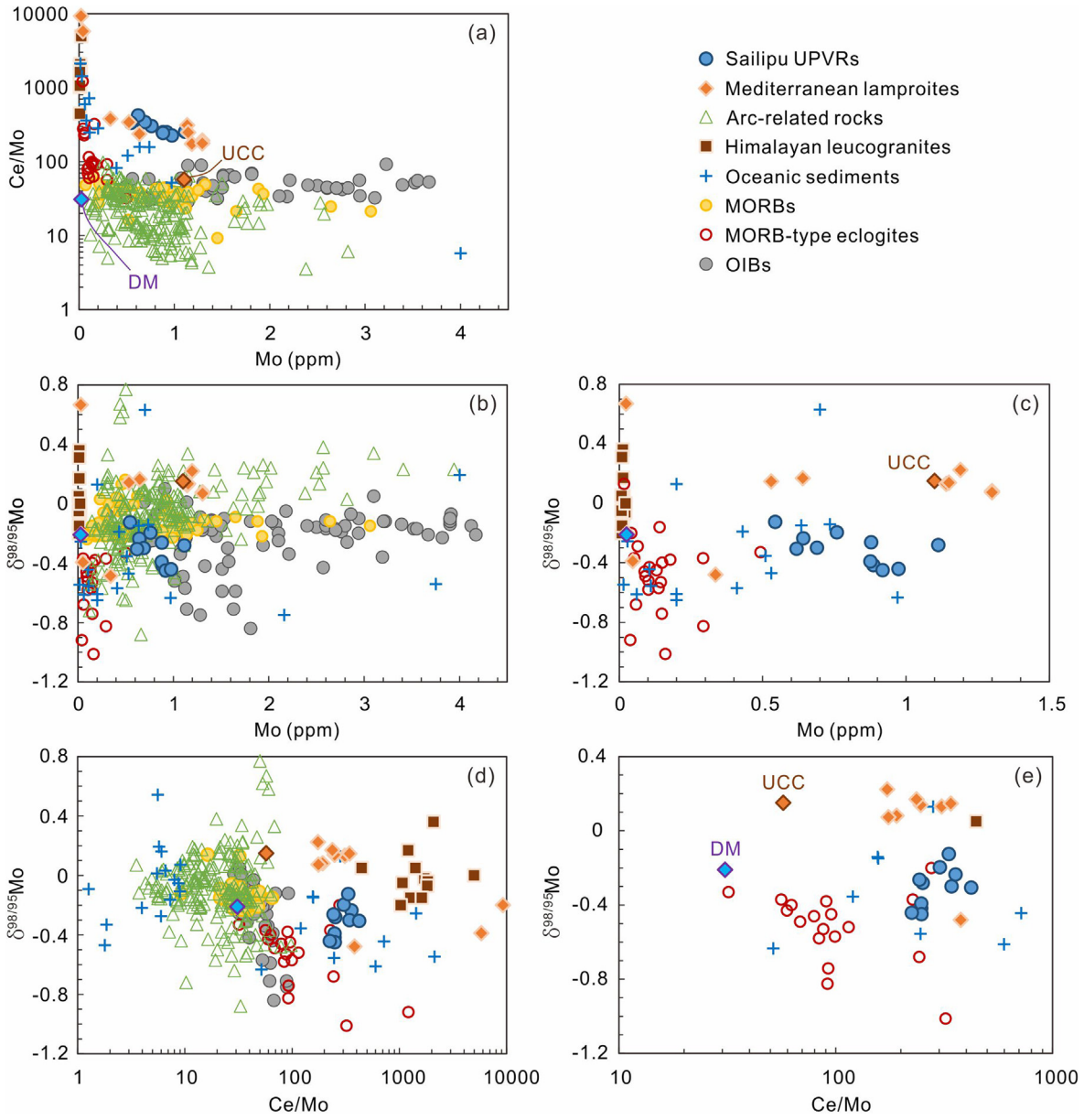

Fig. 5. Plots of (a) Mo versus Ce/Mo ratios, (b, c) Mo versus $\delta^{98/95}$Mo and (d, e) Ce/Mo versus $\delta^{98/95}$Mo for the Sailipu UPVRs and other terrestrial rock types. Data sources: Mediterranean lamproites (Casalini, 2018; Casalini et al., 2019), MORBs (Bezard et al., 2016; Chen et al., 2022b; Liang et al., 2017; McCoy-West et al., 2019), MORB-type eclogites (Ahmad et al., 2021; Chen et al., 2019), OIBs (Bezard et al., 2016; Gaschnig et al., 2021a; Gaschnig et al., 2021b; Liang et al., 2017; Yang et al., 2015), Oceanic sediments (Ahmad et al., 2021; Freymuth et al., 2016; Gaschnig et al., 2017), Himalayan leucogranites (Fan et al., 2021), arc-related rocks as in Fig. 2, upper continental crust (UCC) (Greber et al., 2014; Rudnick and Gao, 2014; Voegelin et al., 2014; Willbold and Elliott, 2017; Yang et al., 2017), depleted mantle (DM) (Bezard et al., 2016; Salters and Stracke, 2004; Willbold and Elliott, 2017).

2021), as the Fe–Ti oxide-rich rocks have lighter $\delta^{98/95}$Mo values than the feldspar-rich rocks. This implies that Fe–Ti oxides have lighter $\delta^{98/95}$Mo values than silicate minerals, if all these phases are from a common parental anhydrous magma (Nebel-Jacobsen et al., 2021). In the case of the Sailipu UPVRs, high Fe_2O_3T (5.85–6.75 wt. %) and TiO_2 (1.37–1.57 wt. %) contents suggest that fractionation of Fe–Ti oxides was negligible. The moderate SiO_2 contents (52.86–55.79 wt. %) and high Mg# values (67.1–72.5; Table 1), as well as the presence of olivine phenocrysts in the Sailipu UPVRs (Fig. S1), suggest that olivine and/or clinopyroxene may have been the main fractionating phase(s). However, because of the lack of appropriate lattice sites, the partition coefficients (D) for Mo between olivine or augite and basaltic melts are 0.01–0.03 (Greaney et al., 2017) or lower (< 0.01; Leitzke et al., 2016, 2017). The relatively uniform Mo contents of peridotites and pyroxenites with variable degrees of fertility also indicate limited Mo partition into dominant silicate mineral phases (Wang and Becker, 2018). Therefore, olivine and/or pyroxene fractionation would not have significantly changed the Mo contents and $\delta^{98/95}$Mo values.

A study of water-rich calc-alkaline basalts to rhyolites from the Aegean Arc identified $\delta^{98/95}$Mo variations of up to 0.3‰, which were assumed to have resulted from magmatic differentiation (Voegelin et al., 2014). Voegelin et al. (2014) showed that amphibole crystallized from the magmas preferentially incorporated isotopically light Mo, with $\Delta^{98/95}Mo_{melt-mineral} \geq 0.5‰$. The fractionation and subsequent removal of amphibole was therefore suggested as an explanation for the isotopically heavy Mo in the

continental crust (Wille et al., 2018). However, the Sailipu UPVRs have isotopically lighter Mo than the mantle and exhibit no correlation between $\delta^{98/95}$Mo values and Dy/Yb ratios, which is inconsistent with amphibole fractionation.

Molybdenum is a chalcophile element under reducing conditions, with $D_{Mo}^{sulfide/melt}$ values of 0.14–5.1 (Li and Audétat, 2012). Leaching experiments on basalts suggest that magmatic sulfides have higher Mo contents and heavier $\delta^{98/95}$Mo values than coexisting silicates (Voegelin et al., 2012). Removal of significant amounts of sulfides would substantially change the Mo contents of residual melt (Willbold and Elliott, 2017) and produce an inverse correlation between Cu/Mo ratios and $\delta^{98/95}$Mo values. However, no such correlation is observed (Fig. 6). Moreover, the fractionation of a minor amount of sulfides does not strongly affect the Mo contents and $\delta^{98/95}$Mo values of silicate melts (Greaney et al., 2018; Li and Audétat, 2012). Therefore, negligible Mo isotopic variations were caused by magmatic differentiation of the Sailipu UPVRs.

5.2.3. Partial melting

Previous studies have proposed that different degrees of partial melting of the mantle might result in Mo isotopic fractionation (Liang et al., 2017; McCoy-West et al., 2019). Large-degree (10–15%) partial melts of the depleted mantle (i.e., MORBs) have slightly heavier $\delta^{98/95}$Mo values than the average chondritic value (−0.14‰ ± 0.02‰), and thus Liang et al. (2017) suggested that Mo isotopic fractionation is limited ($\Delta^{98/95}$Mo < 0.15‰) during moderate degrees of partial melting. The Sailipu UPVRs have large $\delta^{98/95}$Mo variations of 0.32‰, which cannot be due to variable degrees of mantle melting.

The Sailipu UPVRs exhibit large light REE/heavy REE fractionation ($[La/Yb]_N$ = 23.1–39.8; Table S1), consistent with low-degree (< 10%) melting of a mantle source (Guo et al., 2013; Miller et al., 1999). Because Mo^{6+} is more incompatible and has a higher mean coordination number than Mo^{4+} (Leitzke et al., 2017), low-degree partial melts will have higher Mo^{6+}/(total Mo) ratios and heavier Mo isotopes than the mantle residue (McCoy-West et al., 2019). No correlation is evident between $(La/Yb)_N$ and $\delta^{98/95}$Mo (Fig. 7), and the lighter $\delta^{98/95}$Mo values of the Sailipu UPVRs compared with the mantle (Fig. 5b) preclude the possibility that Mo isotopic fractionation was controlled by the degree of partial melting.

Based on the uniform Ce/Mo ratios of diverse terrestrial samples, it has been inferred that bulk $D_{Mo}^{solid/liquid}$ is similar to those of the light REEs, such as Ce (Newsom and Palme, 1984). The Sailipu UPVRs have much higher Ce/Mo ratios (225–422; Fig. 5a) than MORBs (~34; Gale et al., 2013) and OIBs (29–92; Gaschnig et al., 2021a, 2021b; Liang et al., 2017; Yang et al., 2015). They also have high MgO contents (>6 wt. %) and Mg# values (>65) (Table S1) and represent near-primary magmas. Such primitive melt compositions

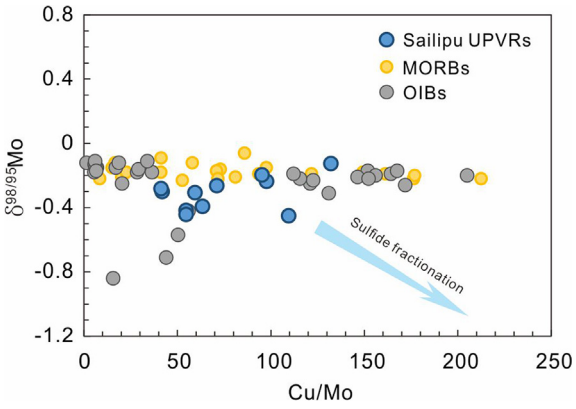

Fig. 6. Plots Cu/Mo versus $\delta^{98/95}$Mo for the Sailipu UPVRs with oceanic basaltic rocks. Data sources for MORBs and OIBs as in Fig. 5.

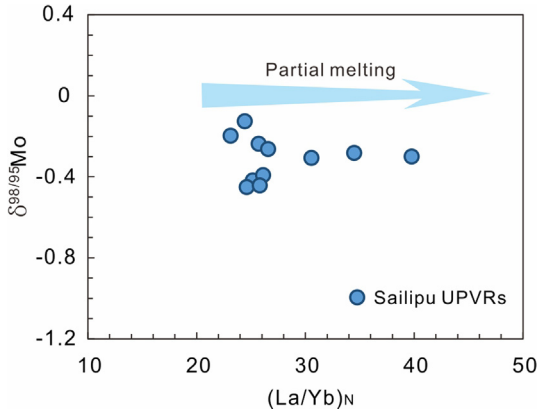

Fig. 7. Diagram of $(La/Yb)_N$ versus $\delta^{98/95}$M for the Sailipu UPVRs. N represent chondrite normalized (Sun and McDonough, 1989).

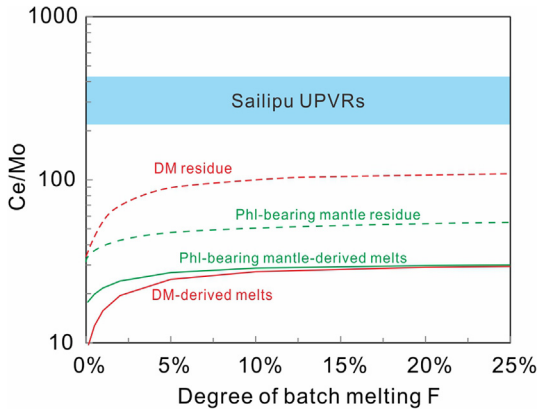

Fig. 8. Variations of Ce/Mo in melts and residues during batch melting of depleted mantle (Salters and Stracke, 2004) and a hypothetical phlogopite (Phl)-bearing mantle sources. The source mineral proportions and partition coefficients used and are given in supplementary Tables S3.

can be modelled using a simple batch-melting approach (Zou, 1997). We used this model to constrain the Ce/Mo ratios of increasing degrees of partial melts of a depleted mantle source (Fig. 8), based on $D_{Mo}^{mineral/melt}$ values from experimental studies (Adam and Green, 2006; Hill et al., 2000; Li and Audétat, 2012; Mckenzie and Onions, 1991; Salters and Longhi, 1999; Voegelin et al., 2014). The initial Ce (772 ppb) and Mo (25 ppb) contents and mineral proportions in the source were assumed to be comparable to the depleted MORB mantle source (Salters and Stracke, 2004), and the bulk D_{Ce} and D_{Mo} used were 0.021 and 0.0115, respectively (Table S3). This implies that Mo is more incompatible than Ce during partial melting, as is evident from the decreasing Ce/Mo ratios (50–36) during the magmatic evolution of the Hekla volcanic suite, Iceland (Yang et al., 2015). Consequently, changing the partition coefficients and initial Mo and Ce contents will not change the main inferences from the modelling.

The modelling results show that melts formed at any degree of partial melting have lower Ce/Mo ratios than those of their mantle source, implying that partial melting could not result in high melt Ce/Mo ratios (Fig. 8). With increasing melting, although the Ce/Mo ratios of the source residue increase and become constant (Fig. 8), the ratios are still much lower than those of the Sailipu UPVRs. Remelting of such residues with high Ce/Mo ratios would produce melts with high Ce/Mo ratios. However, such melts would have very low Ce and Mo contents, and the Sailipu UPVRs have comparable Mo contents to those of MORB (Fig. 5; 0.07–1.93 ppm; Bezard

et al., 2016; Chen et al., 2022b). As such, remelting of the source residue could not have formed the Sailipu UPVRs.

Previous studies have suggested that the Sailipu UPVRs were sourced from a phlogopite-bearing lithospheric mantle source, based on elemental and Sr–Nd–Pb–Os isotope data (Guo et al., 2013; Huang et al., 2015; Liu et al., 2011; Miller et al., 1999). The $D_{Mo}^{phlogopite/melt}$ value has not yet been determined, but if the Mo partitioning behavior of mica group minerals is similar, we can assume it is similar to that of biotite (Table S3; Voegelin et al., 2014). The batch melting model shows that a small amount (3%) of phlogopite in the mantle source would cause a slight increase in Ce/Mo ratios in the melt and an abrupt decrease in the residue (Fig. 8). These values are still lower than the Ce/Mo ratios of the Sailipu UPVRs (225–422; Fig. 8).

Residual refractory Mo-bearing phases (e.g., sulfides and rutile) with heavier Mo isotopes might explain the light $\delta^{98/95}$Mo values of the Sailipu UPVRs. Mass balance calculations indicate that magmatic sulfides have heavier $\delta^{98/95}$Mo values than silicate melts (Voegelin et al., 2012). The degree of mantle melting (<10%) for the formation of the Sailipu UPVRs is not sufficiently high for such sulfides to be totally consumed in the depleted mantle (12%–16%; e.g., Luguet et al., 2003). When melting occurs, the Ce/Mo ratio of mantle-derived magmas would be affected by the coexisting sulfide. The Ce/Mo ratios of some ultramafic xenoliths are lower than those of basaltic rocks, which is also consistent with the presence of residual sulfides (Liang et al., 2017). As such, an inverse correlation between melt Ce/Mo ratios and $\delta^{98/95}$Mo values would be expected if residual sulfide remained in the mantle source. A broad positive correlation (R^2 = 0.27) exhibited by the Sailipu UPVRs exists between Ce/Mo ratios and $\delta^{98/95}$Mo values (Fig. 5d), implying that sulfides do not control the Mo contents and $\delta^{98/95}$Mo values. Moreover, partitioning experiments between monosulfide solid solutions and basaltic melts have indicated that Mo is typically moderately compatible, but that it is very compatible in reducing environments (Li and Audétat, 2012; Skora et al., 2017). A recent study of mantle xenoliths entrained by UPVRs from the Lhasa Terrane showed that the mantle was moderately oxidized (ΔFMQ = 0.5–1.2; Li et al., 2020). These conditions are not ideal for sulfide stability and preclude the presence of residual sulfides in the mantle source of the UPVRs.

In summary, the high Ce/Mo ratios and isotopically light Mo of the Sailipu UPVRs are not related to magmatic processes, including fractional crystallization of olivine ± clinopyroxene and partial melting, and thus must be attributed to the addition of a high-Ce/Mo and isotopically light Mo component to the mantle source.

5.3. Origin of the high-Ce/Mo and isotopically light Mo component

5.3.1. Lower continental crust

Recycled crustal materials have been invoked to have contributed to the formation of UPVRs (Conticelli et al., 2007; Liu et al., 2014), given their relatively high SiO_2 contents (up to 63 wt. %; Guo et al., 2015; Wang et al., 2014; Zhao et al., 2009) and enriched Sr–Nd isotopic compositions (Fig. 4a). Although Mo content and isotope data have not been reported for the southern Tibetan lower crust, the Ce/Mo ratio of average lower continental crust (Ce/Mo = 33; Rudnick and Gao, 2014) is markedly lower than those of the Sailipu UPVRs. Simple mass balance calculations show that the $\delta^{98/95}$Mo value of the average lower continental crust should be −0.4‰ if the upper continental crust has a $\delta^{98/95}$Mo value of 0.14‰ (Greber et al., 2014; Voegelin et al., 2014) and the proportion of upper to lower crust is 1:1 (Yang et al., 2017). A $\delta^{98/95}$Mo value of −0.4‰ for the lower crust is comparable to the lightest $\delta^{98/95}$Mo value of the studied UPVRs (−0.45‰), suggesting a high proportion of crustal material would be required because of the similar Mo contents of the lower crust (~0.6 ppm) and the Sailipu UPVRs (0.54–1.11 ppm). Input of such a large amount of lower crustal material would result in very low Mg# values (< 60), which is inconsistent with those of the Sailipu UPVRs (67.1–72.5). Given that subducting slab-derived fluids would introduce heavier Mo isotopes into the continental crust (Freymuth et al., 2015), the $\delta^{98/95}$Mo values of the lower continental crust should be greater than the calculated value of −0.4‰. In addition, the negligible Mo isotopic fractionation between basaltic and silicic igneous rocks (Gaschnig et al., 2021a) also suggests that the lower crust has similar $\delta^{98/95}$Mo values to the upper crust.

Fan et al. (2021) reported that partial melts generated by crustal anatexis (i.e., leucogranites) in the Himalayan terrane, south of the Tibetan Plateau, have extremely high Ce/Mo ratios (445–4955; Fig. 5). The Sailipu UPVRs have $\delta^{98/95}$Mo and Ce/Mo values that are intermediate between those of MORB-type eclogites and leucogranites (Fig. 5d), indicating crustal melts may have been added to their mantle source. However, the leucogranites have much lower Mo contents (0.008–0.022 ppm) than the Sailipu UPVRs (0.54–1.11 ppm; Figs. 5a–b) and could not have controlled the Mo isotopic systematics of the UPVRs. Moreover, the high Mg# values (67.1–72.5; Table 1) and high incompatible trace element contents of the Sailipu UPVRs are inconsistent with the involvement of a lower crustal component.

5.3.2. Dehydrated oceanic crust

Variable Ce/Mo ratios of arc volcanic rocks have generally been attributed to the fractionation of these two elements during slab dehydration, with Mo entering fluids and being transferred to the mantle wedge more efficiently than Ce. This process results in slab residues with low Mo contents and high Ce/Mo ratios (Bali et al., 2012; Freymuth et al., 2015; Liu et al., 2022b; Skora et al., 2017; Villalobos-Orchard et al., 2020). If this scenario is correct, then the Ce/Mo ratios of subducted oceanic crust would be higher than those of MORBs. Hybrid melts between those derived from subducted oceanic crust and deep mantle (e.g., OIBs) would also have high Ce/Mo ratios. Although the Ce/Mo ratios of OIBs (29–92) are higher than those of most arc igneous rocks (3.5–97.6; Fig. 5d), these are still much lower than those of the Sailipu UPVRs (225–422). The Sailipu UPVRs also have lower Mo contents than most OIBs (0.3–16 ppm; Gaschnig et al., 2021b; Liang et al., 2017; Yang et al., 2015), suggesting they have different mantle sources.

The fluids released by subducting oceanic crust are enriched in heavy Mo isotopes, and lighter Mo isotopes remain in slab residue (Freymuth et al., 2015; König et al., 2016; Villalobos-Orchard et al., 2020; Willbold and Elliott, 2017). The heavy $\delta^{98/95}$Mo values of Mariana and Izu arc volcanic rocks have been suggested to record metasomatism by slab-derived fluids (Freymuth et al., 2015; Villalobos-Orchard et al., 2020). As such, the subducted oceanic crust has high Ce/Mo and light $\delta^{98/95}$Mo values. Based on the Mo isotope balance between arc magmas and subducted oceanic crust, the residual slab transported into the deeper mantle beneath the Mariana and Izu arcs has $\delta^{98/95}$Mo values of −0.27‰ to −0.36‰ and − 0.35‰, respectively (Freymuth et al., 2015; Villalobos-Orchard et al., 2020). Recent studies have shown that MORB-type eclogites (i.e., recycled oceanic crust) also have very light $\delta^{98/95}$Mo values of −1.01‰ to −0.74‰ (Ahmad et al., 2021) or −0.68‰ to −0.13‰ (Chen et al., 2019). This recycled oceanic crust (±oceanic sediments) with light Mo isotopes and high Ce/Mo ratios has been proposed as the source of EM1-type basalts in northeast China (Ma et al., 2022) and adakitic andesites in northwest China (Zhang et al., 2020). It appears that recycled, dehydrated oceanic crust subducted into the deep mantle would have much lighter $\delta^{98/95}$Mo values (OIB values as light as −0.84‰; Fig. 5d; Gaschnig et al., 2021b) than MORB, which is consistent with the light $\delta^{98/95}$Mo values of the Sailipu UPVRs. Dehydrated oceanic crust generally has low contents of Mo (0.038–

0.493 ppm; mean = 0.15 ppm; Chen et al., 2019; Ahmad et al., 2021) and other incompatible trace elements and MORB-like Sr–Nd–Hf isotopic compositions (Fig. 4a). As such, a high proportion of dehydrated oceanic crust would be required to obtain the light $\delta^{98/95}$Mo values of the studied UPVRs. However, the Sailipu UPVRs have highly enriched Sr–Nd–Hf isotopic compositions and elevated trace element contents, which are inconsistent with dehydrated oceanic crust being the predominant component in their source.

5.3.3. Sediments

Subduction can transport sediments (including terrigenous and marine sediments) into the mantle, thus possibly modifying the Mo contents and $\delta^{98/95}$Mo values of mantle-derived melts. Most sediment types have similar Sm/Nd ratios, but Lu/Hf ratios vary markedly owing to zircon-controlled fractionation (Patchett et al., 1984). Terrigenous sediments typically have high Hf/Sm (> 0.7; Gasperini et al., 2002) and low $^{176}Hf/^{177}Hf$ ratios, whereas the opposite is true for oceanic sediments (Vervoort et al., 2011). Melts mixed with continental sediments plot below the Nd–Hf isotope terrestrial array (Fig. 4b). However, the Sailipu UPVRs have high $\varepsilon_{Hf}(t)$ values at a given $\varepsilon_{Nd}(t)$ value and low Hf/Sm ratios (0.38–0.46; Table S1), which are inconsistent with the involvement of terrigenous sediments. In general, continental margin sediments have heavy Mo isotopes because of the reducing depositional conditions and high primary oceanic productivity (Kendall et al., 2017). Therefore, such sediments are not suitable candidates for the source of isotopically light Mo. Moreover, terrigenous sediments have Nb/Ta ratios of 12.5 ± 1.8 (Barth et al., 2000), and the super-chondritic Nb/Ta ratios (18.9–20.8) of the Sailipu UPVRs are inconsistent with a contribution from such sediments.

Recycling of marine carbonates and black shales into the mantle can modify the composition of mantle-derived magmas (Freymuth et al., 2016; Li et al., 2017). These carbonates may directly record seawater $\delta^{98/95}$Mo values and are characterized by heavy $\delta^{98/95}$Mo values (1.43‰ ± 0.97‰; Kendall et al., 2017; Romaniello et al., 2016). Black shales generally have heavier $\delta^{98/95}$Mo values (0.52–2.00‰; Freymuth et al., 2016) than the depleted mantle. Contributions from marine carbonates or black shales to the mantle would result in magmas having relatively heavier $\delta^{98/95}$Mo values than the depleted mantle. For example, Zhang et al. (2020) suggested that normal arc andesites with heavy $\delta^{98/95}$Mo values of 0.33‰–1.08‰ were derived from a marine carbonate-modified mantle source. Carbonate rocks and black shales have variable Mo contents with sub-crustal abundances (≪ 1 ppm; Kendall et al., 2017) and 40–50 ppm (Freymuth et al., 2016), respectively. However, they both have low Ce/Mo ratios (<30; Freymuth et al., 2016; Zhang et al., 2020), which are inconsistent with the Ce/Mo and Mo isotopic variations of the Sailipu UPVRs. In addition, carbonates have significantly less radiogenic Sr ($^{87}Sr/^{86}Sr \sim 0.709$; Fietzke et al., 2008) and could not have contributed to the formation of the Sailipu UPVRs ($^{87}Sr/^{86}Sr_i$ = 0.725012–0.727457).

Other marine sediment samples from several ocean drilling sites have variable $\delta^{98/95}$Mo values, and some pelagic sediments have very light $\delta^{98/95}$Mo values of −1.87‰ (Fig. 5b; Freymuth et al., 2015). König et al. (2016) attributed the light $\delta^{98/95}$Mo values of Papua New Guinean and Cypriot volcanic rocks to an increasing contribution from sediment melts, which also increased the Ce/Mo ratios. The $\delta^{98/95}$Mo values of volcanic rocks from the Martinique and Lesser Antilles arcs changed from −0.15‰ to 0.08‰ and from −0.06‰ to –0.88‰ at 7 Ma, respectively, which has been explained as recording the transition from black shale to marine sediment contributions during subduction (Gaschnig et al., 2017). The high Ce/Mo ratios of the sediment components in these arc magmas reflect an increased contribution from low-CaO clay minerals. Gaschnig et al. (2017) further suggested that marine sediments were the primary source of isotopically light Mo in igneous rocks, and that Mo isotopic fractionation during its isolation from the oceanic crust was not required. Casalini et al. (2019) determined the Ce/Mo ratios and $\delta^{98/95}$Mo values of potassic igneous rocks and sediments from central–southern Italy and suggested that the sediment-dominated arc rocks inherited the high Ce/Mo ratios and $\delta^{98/95}$Mo values of subducted marine sediments. In particular, the high Ce/Mo ratios (170–350; Fig. 5a; Casalini et al., 2019) of the UPVRs in central Italy were inferred to have resulted from metasomatism by Ca-poor sediments of the mantle source. Ahmad et al. (2021) investigated Mn oxide-rich pelagic sediments from the western Alps, which might represent subducted pelagic sediments on Tethyan oceanic crust. These Mn-rich pelagic sediments with low CaO contents (0.52–6.01 wt. %) have light $\delta^{98/95}$Mo values (−0.26‰ to −1.50‰) and high Ce/Mo ratios (82–2124), similar to those of the Sailipu UPVRs (Fig. 5). Therefore, the high Ce/Mo ratios and light $\delta^{98/95}$Mo values of the Sailipu UPVRs probably represent a mantle source modified by low-CaO pelagic sediments. The incorporation of recycled Tethyan sediments into the mantle source can also explain the high Th/U ratios and radiogenic Pb–Nd of the UPVRs on the southern Tibetan Plateau (Gao et al., 2007), as well as the light $\delta^{98/95}$Mo values of the UPVRs in the Western Alps (Casalini, 2018).

5.4. Source of the Sailipu UPVRs

The Sailipu UPVRs have light REE contents that are several times higher than those of the continental crust; they also have high Th contents (198–361 ppm) and Th/La ratios of 2.6–3.4 (Figs. 2d and 3b; Table S1). The light REE and Th contents of partial melts increase when a suitable host mineral is absent or exhausted in the mantle source. Thorium and light REE are generally hosted by carbonate and accessory mineral phases including monazite, apatite, and epidote-group minerals (Hermann, 2002; Hermann and Rubatto, 2009; Skora et al., 2015, 2017). The high Ce/Mo ratios and light $\delta^{98/95}$Mo values of the Sailipu UPVRs were probably inherited from low-CaO pelagic sediments. Monazite is a plausible host for the light REEs (especially Ce) and Th in CaO-poor sediments. The high Ce contents (> 100 ppm) and Th/La ratios (1.36–2.59) of partial melts of monazite-bearing sediments (e.g., Hermann and Rubatto, 2009) are similar to those of the Sailipu UPVRs. These UPVRs with high Th/La ratios differ from subduction-related magmas (Th/La < 0.4; Plank, 2005). Another potential mineral with high Th/La ratios is lawsonite, which incorporates Th, U, Sr, Pb, and light REEs (e.g., Martin et al., 2014; Wang et al., 2019). High-Th/La melts are generated when lawsonite is consumed. Wang et al. (2021) proposed that partial melting of lawsonite blueschists at shallow mantle depths may form high-Th/La UPVRs. These observations suggest that monazite and/or lawsonite are likely the predominant accessory phases in the source of the Sailipu UPVRs.

However, the light $\delta^{98/95}$Mo values cannot be explained by monazite and lawsonite, as these minerals do not contain significant Mo (e.g., Skora et al., 2017). Given that Mo^{4+} is preferentially incorporated into rutile because of its favorable ionic radius and valence (Bali et al., 2012), rutile should have high Mo contents and light Mo isotopes (Freymuth et al., 2015; Greaney et al., 2017; König et al., 2016). Chen et al. (2019) showed that rutile has high Mo contents (2.44–5.30 ppm) and light $\delta^{98/95}$Mo values (−1.2‰ to −0.31‰). Equilibrium melts with residual rutile would have heavier Mo isotopes than their mantle source, which is inconsistent with the light $\delta^{98/95}$Mo values of the Sailipu UPVRs (−0.45‰ to −0.13‰). However, rutile is typically unstable in the mantle due to its high solubility in basaltic magmas (Xiong et al., 2009), which exhausts rutile and results in melts with light $\delta^{98/95}$Mo values due to the high $D_{Mo}^{rutile/melt}$ value (~4; Skora et al., 2017). The Sailipu UPVRs have much lower Mo contents (0.54–1.11 ppm) than rutile,

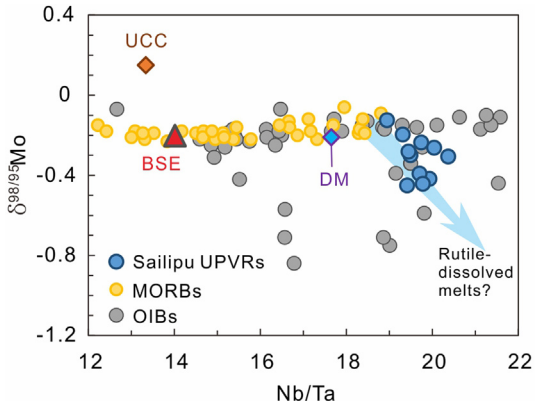

Fig. 9. Diagram of Nb/Ta versus $\delta^{98/95}$Mo for the Sailipu UPVRs with oceanic basaltic rocks. Data sources: bulk silicate earth (BSE) (Burkhardt et al., 2014; Greber et al., 2015; Palme and O'Neill, 2014), others as in Fig. 5.

and the breakdown of even small amounts (< 5%) of rutile would abruptly change the $\delta^{98/95}$Mo values of such melts (Guo et al., 2013; Williams et al., 2004).

This inference is also consistent with the Nb/Ta ratios (18.9–20.8; Fig. 9) of the Sailipu UPVRs. Rutile strongly incorporates Nb and Ta ($D^{rutile/melt}_{Nb,\ Ta} \gg 1$) and also substantially fractionates Nb from Ta ($D^{rutile/melt}_{Nb/Ta} < 1$; e.g., Xiong et al., 2005). Melts in equilibrium with rutile are expected to have high Nb/Ta ratios and negative Nb–Ta anomalies in primitive mantle-normalized trace element patterns, consistent with those observed for the Sailipu UPVRs. Progressive melting that then exhausts rutile likely results in lower Nb/Ta ratios (e.g., Liu et al., 2008; Xiong et al., 2009). However, the limited amount of rutile dissolved in the melt does not substantially change the melt Nb/Ta ratios because of its low Nb and Ta contents. In addition, the K_2O contents of the UPVRs are nearly constant (6–8 wt. %; Table S1), indicative of a phlogopite-bearing mantle source (Foley et al., 1987; Guo et al., 2013; Huang et al., 2015; Miller et al., 1999; Prelevic et al., 2012; Williams et al., 2004). Phlogopite has been found in mantle xenoliths in the Sailipu area (Cheng and Guo, 2017; Liu et al., 2011), suggesting that it exerts a control on the geochemistry of the UPVRs. Ionov and Hofmann (1995) reported that phlogopite from mantle xenoliths has super-chondritic Nb/Ta ratios (19.2–54) and very high Nb contents (up to 711 ppm). Phlogopite breakdown during melting would increase the Nb/Ta ratios of the UPVRs, which would likely compensate for the low Nb/Ta effect caused by rutile melting. As shown in Fig. 9, the Sailipu UPVRs plot between the field for depleted MORB and a component with lighter $\delta^{98/95}$Mo values and higher Nb/Ta ratios. The former represents a depleted mantle source that produces high Mg# values (~70) and Cr and Ni contents, and the latter represents a significant contribution from metasomatic materials with light $\delta^{98/95}$Mo values and high Ce/Mo, Nb/Ta, and Th/La ratios (Fig. 10).

5.5. Geodynamic setting of the Sailipu UPVRs

The Sailipu UPVRs were generated during the post-orogenic stage of the India–Asia continental collision, and the light-$\delta^{98/95}$Mo components in their mantle source must be exotic in origin. As proposed by Tommasini et al. (2011) and Casalini et al. (2021) for the Mediterranean lamproites, we invoke a two-stage model for formation of the Sailipu UPVRs. First, ancient oceanic subduction in the Paleo-, meso-, and NeoTethys oceans introduced Ca-poor pelagic sediments ± oceanic crust into the inner parts of the overlying subcontinental lithospheric mantle (i.e., the southern Tibetan lithosphere). This formed metasomatic vein components consisting of rutile + monazite ± lawsonite in the lithospheric mantle (Fig. 10a). The Th/La and Ce/Mo ratios are not correlated with K_2O contents (Fig. S6), suggesting that the K-rich phase (i.e., phlogopite) was not related to this type of metasomatism. During oceanic subduction, the reaction between oceanic crust- and/or sediment-derived melts and the ambient lithosphere formed another lithology in the lithospheric mantle, such as phlogopite-bearing peridotite and pyroxenite (Huang et al., 2015), which have been observed as xenoliths in the Sailipu UPVRs (Cheng and Guo, 2017; Liu et al., 2011).

During the post-orogenic stage, ongoing lithospheric thickening and thermal disturbance was caused by convective thinning of the lithospheric mantle (e.g., Liu et al., 2011; Turner et al., 1996), which eventually resulted in partial melting of the metasomatized mantle. Given that pyroxenite has a lower solidus temperature than peridotite (e.g., Hirschmann et al., 2003), initial melting and exhaustion of pyroxenite would have formed melts with radiogenic Os isotopes, as is the case for the southern Tibetan UPVRs (Huang et al., 2015; Wang et al., 2014). Further lithospheric extension and thermal relaxation would have increased the geothermal gradient (Liu et al., 2011). Such a high mantle temperature (e.g., 1069–1249 °C; Liu et al., 2011) resulted in total consumption and melting of the vein components consisting of rutile + monazite ± l awsonite, which produced hybrid melts with high Ce/Mo and Th/La ratios and light Mo isotopes ($\delta^{98/95}$Mo ≤ −0.45‰; Fig. 10b). As such, the geochemical and isotopic variability of the Sailipu UPVRs can be explained by mixing of melts generated from multiple mantle domains, including phlogopite-bearing peridotite, pyroxenite, and metasomatic vein components consisting of rutile + monazite ± lawsonite.

5.6. A light Mo isotopic reservoir in the Tethyan lithospheric mantle?

The estimated $\delta^{98/95}$Mo value of the BSE is −0.21‰ ± 0.06‰ (Burkhardt et al., 2014; Greber et al., 2015; Liang et al., 2017), which is lighter than the estimated values for the upper continental crust (0.05–0.15‰; Chen et al., 2022a; Greber et al., 2014; Voegelin et al., 2014; Yang et al., 2017). Although the Mo isotopic compositions of the middle and lower continental crust are not well defined, we assume these are comparable to those of the upper continental crust because of the limit Mo isotopic fractionation during partial melting and fractional crystallization (Chen et al., 2022a; Gaschnig et al., 2021a; Yang et al., 2015). Therefore, there is a clear Mo isotopic difference between the continental crust and BSE. Given that shallow asthenospheric mantle-derived melts (i.e., MORBs) have similar $\delta^{98/95}$Mo values to the BSE, an isotopically light Mo reservoir may exist in Earth's deep mantle. This reservoir has been speculated to be subducted slabs that have accumulated in either the mantle transition zone (Li et al., 2019; Ma et al., 2022) or at the core–mantle boundary (Liang et al., 2017). Some OIBs derived from the deep mantle have very light $\delta^{98/95}$Mo values (−0.84‰; Gaschnig et al., 2021b), whereas the average $\delta^{98/95}$Mo value of all published OIB data is −0.22‰ ± 0.04‰ (2SE; n = 87; Gaschnig et al., 2021a, 2021b; Liang et al., 2017; Yang et al., 2015), which overlaps with that of the depleted mantle (−0.21‰ ± 0.02‰; Bezard et al., 2016).

Our study suggests that a light Mo isotopic reservoir exists in the lithospheric mantle beneath the southern Tibetan Plateau, thus explaining the $\delta^{98/95}$Mo offset between the continental crust and the BSE. This reservoir is an end-member that contains rutile, monazite, and/or lawsonite. Rutile has been found in mica–amphibole–rutile–ilmenite–diopside (MARID)-type cratonic mantle xenoliths (Förster et al., 2018) and can survive for tens of millions of years in the lithospheric mantle (e.g., Konzett et al., 1998). In metasomatized lithospheric mantle, the metasomes may be isolated in veins or occur as intergranular layers (e.g., Foley, 1992). Therefore, these metasomatic components formed during oceanic subduction, as

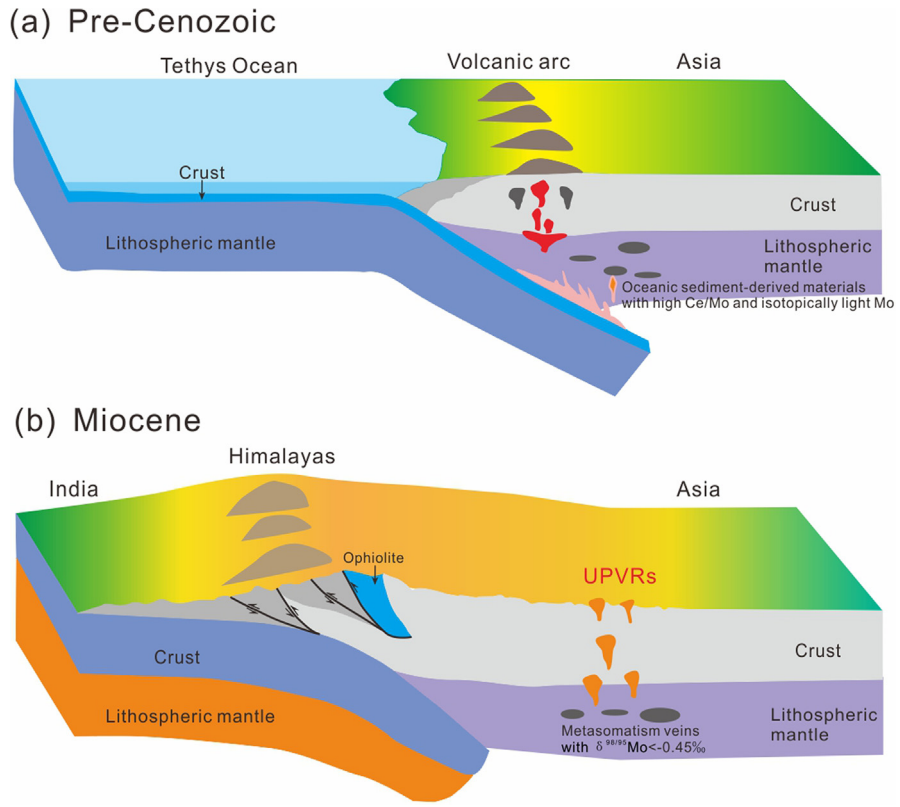

Fig. 10. Two-phase reconstructions of the geodynamic process for the formation of the southern Tibetan UPVRs. (a) oceanic sediment metasomatism during the subduction of the Tethyan lithosphere to form a veined component (consists of rutile + monazite ± lawsonite) with high Ce/Mo and Th/La ratios, and light $\delta^{98/95}$Mo. (b) During the Miocene, a high mantle temperature resulted in the total consumption and melting of the veined components, produced the hybrid melts represented by the southern Tibetan UPVRs.

the Ce/Mo ratios and Mo isotopic compositions were inherited mainly from low-CaO pelagic sediments. This metasomatism by sediments during oceanic subduction forms isotopically lighter Mo in the mantle.

The UPVRs on the southern Tibetan Plateau and orogenic lamproites in the Mediterranean region have similar elemental and Sr–Nd isotopic compositions (Figs. 2–3 and S3; Casalini et al., 2021; Gao et al., 2007; Tommasini et al., 2011; Wang et al., 2021) and, in particular, anomalously high Th/La ratios (>0.5). Tommasini et al. (2011) suggested an exotic component with high Sm/La and Th/La ratios (namely SALATHO) stored in the lithospheric mantle for an extended duration (300–500 Myr) was responsible for the high Th/La ratios of the Tethyan UPVRs. This is also consistent with the enriched Sr–Nd–Hf isotopic compositions of the UPVRs (Figs. 4 and 9). The UPVRs in the Tuscan magmatic province of central Italy have high Ce/Mo ratios (173–340), comparable to those of the Sailipu UPVRs (Fig. 5a), which have been attributed to metasomatism by Ca-poor sediments in the mantle source (Casalini et al., 2019). The $\delta^{98/95}$Mo values of these rocks are similar to those of exposed Ca-poor sedimentary rocks (Casalini et al., 2019). The UPVRs from the Western Alps have variable $\delta^{98/95}$Mo values (−0.48‰ to 0.67‰; Casalini et al., 2019), and the heavy $\delta^{98/95}$Mo values are similar to those of fluid-dominated arc igneous rocks. Casalini et al. (2019) suggested that the origin of the light-$\delta^{98/95}$Mo component was uncertain but was likely recycled Tethyan sediments. Given their similar high Th/La and Ce/Mo ratios and light $\delta^{98/95}$Mo values to those of the Sailipu UPVRs (Figs. 2 and 5), we speculate that the UPVRs in the southern Tibetan Plateau and Mediterranean regions were derived from veined lithospheric mantle domains. Therefore, metasomatized vein components in Tethyan lithospheric mantle not only result in distinctive trace element and Sr–Nd–Hf isotopic compositions but also high Ce/Mo ratios and light $\delta^{98/95}$Mo values (Fig. 10). The Tethyan UPVRs occur over a distance of 10,000 km from the Mediterranean region to southern Tibet (Casalini et al., 2021; Gao et al., 2007; Tommasini et al., 2011; Wang et al., 2021) and represents a heterogeneous and isotopically light Mo reservoir in the lithospheric mantle.

6. Conclusions

The Sailipu UPVRs have primitive geochemical characteristics (e.g., high Mg# values), light $\delta^{98/95}$Mo values (−0.45‰ to −0.13‰) and MORB-like Mo contents (0.54–1.11 ppm). High Ce/Mo ratios (225–422) are positively correlated with $\delta^{98/95}$Mo values. Fractionation of mafic or sulfide mineral phases and partial melting of normal mantle cannot explain the Mo isotopic variations. The enriched Sr–Nd isotopic compositions and higher $\varepsilon_{Hf}(t)$ values at a given $\varepsilon_{Nd}(t)$ value compared with the terrestrial array suggest the source of the Sailipu UPVRs contained recycled pelagic sediments. Correlations between Ce/Mo, Nb/Ta, and $\delta^{98/95}$Mo are best explained if the UPVRs are hybrid melts from two mantle end-members. The light Mo isotope end-member is subducted pelagic sediments. The other end-member is depleted mantle with MORB-like $\delta^{98/95}$Mo values. The metasomatic component produced by pelagic sediments consists of several phases (rutile, phlogopite, monazite, and lawsonite), resulting in high Ce/Mo, Nb/Ta, and Th/La ratios. These minerals were preserved in the lithospheric mantle for a protracted period and thus generated the radiogenic Sr–Nd–Hf isotopic compositions of the Sailipu UPVRs. Given that these UPVRs are distributed widely from the Mediterranean region to the southern Tibetan Plateau, we propose that such a reservoir containing isotopically light Mo can explain the different Mo isotopic compositions of the BSE and continental crust.

Declaration of Competing Interest

The authors declare that they have no known competing financial interests or personal relationships that could have appeared to influence the work reported in this paper.

Data availability

Research data is provided in the supplementary material.

Acknowledgements

We thank Professors Jeffrey G. Catalano (the Executive Editor) and Julie Prytulak (the Associate Editor) for patient editorial handling and the three anonymous reviewers for constructive suggestions that have greatly improved the manuscript. We thank Jianbin Wu for his assistance in the field work, Hongxia Yu, Yinhui Zhang, Xianglin Tu, Shengling Sun, Yaqian Wen, Zhao Zhang, Liying Zhang and Changqi Yang for their help in whole-rock chemical analyses. This paper is benefited from the inspiration discussion with Hao Wang, Hongli Li, Xingcheng Liu, Ming Lei and Fanhui Pei, and email communication with Martina Casalini. We thank Yamei Tian for sharing her Mo isotope database on the oceanic basalts. This research was supported by the National Key Research and Development Project of China (Grant No. 2020YFA0714800), the Second Tibetan Plateau Scientific Expedition and Research (STEP) Program (Grant No. 2019QZKK0702), the National Natural Science Foundation of China (Grant No. 41973027, 41730427 and 42121002), and the Fundamental Research Funds for the Central Universities of China (Grant No. 2652019054).

Appendix A. Supplementary material

This file consists of supplementary figures and research data. Supplementary material to this article can be found online at https://doi.org/10.1016/j.gca.2022.11.023.

References

Aarons, S.M., Johnson, A.C., Rader, S.T., 2021. Forming Earth's Continental Crust: A Nontraditional Stable Isotope Perspective. Elements 17, 413–418.
Adam, J., Green, T., 2006. Trace element partitioning between mica- and amphibole-bearing garnet lherzolite and hydrous basanitic melt: 1. Experimental results and the investigation of controls on partitioning behaviour. Contrib. Mineral. Petr. 152, 1–17.
Ahmad, Q., Wille, M., König, S., Rosca, C., Hensel, A., Pettke, T., Hermann, J., 2021. The Molybdenum isotope subduction recycling conundrum: A case study from the Tongan subduction zone, Western Alps and Alpine Corsica. Chem. Geol. 576, 120231.
Bali, E., Keppler, H., Audetat, A., 2012. The mobility of W and Mo in subduction zone fluids and the Mo–W–Th–U systematics of island arc magmas. Earth Planet. Sci. Lett. 351–352, 195–207.
Barth, M.G., McDonough, W.F., Rudnick, R.L., 2000. Tracking the budget of Nb and Ta in the continental crust. Chem. Geol. 165, 197–213.
Bayon, G., Burton, K.W., Soulet, G., Vigier, N., Dennielou, B., Etoubleau, J., Ponzevera, E., German, C.R., Nesbitt, R.W., 2009. Hf and Nd isotopes in marine sediments: Constraints on global silicate weathering. Earth Planet. Sci. Lett. 277, 318–326.
Bezard, R., Fischer-Gödde, M., Hamelin, C., Brennecka, G.A., Kleine, T., 2016. The effects of magmatic processes and crustal recycling on the molybdenum stable isotopic composition of Mid-Ocean Ridge Basalts. Earth Planet. Sci. Lett. 453, 171–181.
Burkhardt, C., Hin, R.C., Kleine, T., Bourdon, B., 2014. Evidence for Mo isotope fractionation in the solar nebula and during planetary differentiation. Earth Planet. Sci. Lett. 391, 201–211.
Casalini, M., 2018. 98Mo/95Mo and 238U/235U in lamproites, shoshonites, and high-K calc-alkaline rocks from Western Alps: inferences on their genesis. Ital. J. Geosci. 137, 465–477.
Casalini, M., Avanzinelli, R., Tommasini, S., Elliott, T., Conticelli, S., 2019. Ce/Mo and Molybdenum Isotope Systematics in Subduction-Related Orogenic Potassic Magmas of Central-Southern Italy. Geochem. Geophys. Geosyst. 20, 2753–2768.
Casalini, M., Avanzinelli, R., Tommasini, S., Natali, C., Bianchini, G., Prelević, D., Mattei, M., Conticelli, S., 2021. Petrogenesis of Mediterranean lamproites and associated rocks: The role of overprinted metasomatic events in the post-collisional lithospheric upper mantle. Geol. Soc. Lond. Spec. Publ. 513, 271–296.
Chen, S., Hin, R.C., John, T., Brooker, R., Bryan, B., Niu, Y., Elliott, T., 2019. Molybdenum systematics of subducted crust record reactive fluid flow from underlying slab serpentine dehydration. Nat. Commun. 10, 4773.
Chen, S., Niu, Y., Gong, H., Wang, X., Xue, Q., 2022a. Re-assessment of the effect of fractional crystallization on Mo isotopes: Constraints from I-type granitoids and their enclosed mafic magmatic enclaves. Chem. Geol. 597, 120814.
Chen, S., Sun, P., Niu, Y., Guo, P., Elliotte, T., Hinf, R.C., 2022b. Molybdenum isotope systematics of lavas from the East Pacific Rise: Constraints on the source of enriched mid-ocean-ridge basalt. Earth Planet. Sci. Lett. 578, 117283.
Chen, J.-L., Xu, J.-F., Zhao, W.-X., Dong, Y.-H., Wang, B.-D., Kang, Z.-Q., 2011. Geochemical variations in Miocene adakitic rocks from the western and eastern Lhasa terrane: Implications for lower crustal flow beneath the Southern Tibetan Plateau. Lithos 125, 928–939.
Cheng, Z., Guo, Z., 2017. Post-collisional ultrapotassic rocks and mantle xenoliths in the Sailipu volcanic field of Lhasa terrane, south Tibet: Petrological and geochemical constraints on mantle source and geodynamic setting. Gondw. Res. 46, 17–42.
Chung, S.L., Liu, D.Y., Ji, J.Q., Chu, M.F., Lee, H.Y., Wen, D.J., Lo, C.H., Lee, T.Y., Qian, Q., Zhang, Q., 2003. Adakites from continental collision zones: Melting of thickened lower crust beneath southern Tibet. Geology 31, 1021–1024.
Conticelli, S., Carlson, R.W., Widom, E., Serri, G., 2007. Chemical and isotopic composition (Os, Pb, Nd, and Sr) of Neogene to Quaternary calc-alkalic, shoshonitic, and ultrapotassic mafic rocks from the Italian peninsula: Inferences on the nature of their mantle sources. In: Beccaluva, L., Bianchini, G., Wilson, M. (Eds.), Cenozoic Volcanism in the Mediterranean Area, 418. Geological Society of America Special Paper, pp. 171–202.
Fan, J.-J., Wang, Q., Li, J., Wei, G.-J., Ma, J.-L., Ma, L., Li, Q.-W., Jiang, Z.-Q., Zhang, L., Wang, Z.-L., Zhang, L., 2021. Boron and molybdenum isotopic fractionation during crustal anatexis: Constraints from the Conadong leucogranites in the Himalayan Block, South Tibet. Geochim. Cosmochim. Acta 297, 120–142.
Fietzke, J., Liebetrau, V., Günther, D., Gürs, K., Hametner, K., Zumholz, K., Hansteen, T.H., Eisenhauer, A., 2008. An alternative data acquisition and evaluation strategy for improved isotope ratio precision using LA-MC-ICP-MS applied to stable and radiogenic strontium isotopes in carbonates. J. Anal. At. Spectrom. 23, 955–961.
Foley, S., 1992. Vein-Plus-Wall-Rock Melting Mechanisms in the Lithosphere and the Origin of Potassic Alkaline Magmas. Lithos 28, 435–453.
Foley, S.F., Venturelli, G., Green, D.H., Toscani, L., 1987. The Ultrapotassic Rocks - Characteristics, Classification, and Constraints for Petrogenetic Models. Earth Sci. Rev. 24, 81–134.
Förster, M.W., Prelević, D., Schmück, H.R., Buhre, S., Marschall, H.R., Mertz-Kraus, R., Jacob, D.E., 2018. Melting phlogopite-rich MARID: Lamproites and the role of alkalis in olivine-liquid Ni-partitioning. Chem. Geol. 476, 429–440.
Freymuth, H., Vils, F., Willbold, M., Taylor, R.N., Elliott, T., 2015. Molybdenum mobility and isotopic fractionation during subduction at the Mariana arc. Earth Planet. Sci. Lett. 432, 176–186.
Freymuth, H., Elliott, T., van Soest, M., Skora, S., 2016. Tracing subducted black shales in the Lesser Antilles arc using molybdenum isotope ratios. Geology 44, 987–990.
Gale, A., Dalton, C.A., Langmuir, C.H., Su, Y.J., Schilling, J.G., 2013. The mean composition of ocean ridge basalts. Geochem. Geophys. Geosyst. 14, 489–518.
Gao, Y.F., Hou, Z.Q., Kamber, B.S., Wei, R.H., Meng, X.J., Zhao, R.S., 2007. Lamproitic rocks from a continental collision zone: Evidence for recycling of subducted Tethyan oceanic sediments in the mantle beneath southern Tibet. J. Petrol. 48, 729–752.
Gaschnig, R.M., Reinhard, C.T., Planavsky, N.J., Wang, X., Asael, D., Chauvel, C., 2017. The Molybdenum Isotope System as a Tracer of Slab Input in Subduction Zones: An Example From Martinique, Lesser Antilles Arc. Geochem. Geophys. Geosyst. 18, 4674–4689.
Gaschnig, R.M., Rader, S.T., Reinhard, C.T., Owens, J.D., Planavsky, N., Wang, X., Asael, D., Greaney, A., Helz, R., 2021a. Behavior of the Mo, Tl, and U isotope systems during differentiation in the Kilauea Iki lava lake. Chem. Geol. 574, 120239.
Gaschnig, R.M., Reinhard, C.T., Planavsky, N.J., Wang, X., Asael, D., Jackson, M.G., 2021b. The impact of primary processes and secondary alteration on the stable isotope composition of ocean island basalts. Chem. Geol. 581, 120416.
Gasperini, D., Blichert-Toft, J., Bosch, D., Del Moro, A., Macera, P., Albarede, F., 2002. Upwelling of deep mantle material through a plate window: Evidence from the geochemistry of Italian basaltic volcanics. J. Geophys. Res.-Sol. Ea. 107.
Greaney, A.T., Rudnick, R.L., Helz, R.T., Gaschnig, R.M., Piccoli, P.M., Ash, R.D., 2017. The behavior of chalcophile elements during magmatic differentiation as observed in Kilauea Iki lava lake, Hawaii. Geochim. Cosmochim. Acta 210, 71–96.
Greaney, A.T., Rudnick, R.L., Gaschnig, R.M., Whalen, J.B., Luais, B., Clemens, J.D., 2018. Geochemistry of molybdenum in the continental crust. Geochim. Cosmochim. Acta 238, 36–54.
Greber, N.D., Pettke, T., Nägler, T.F., 2014. Magmatic–hydrothermal molybdenum isotope fractionation and its relevance to the igneous crustal signature. Lithos 190–191, 104–110.
Greber, N.D., Puchtel, I.S., Nägler, T.F., Mezger, K., 2015. Komatiites constrain molybdenum isotope composition of the Earth's mantle. Earth Planet. Sci. Lett. 421, 129–138.
Guo, Z., Wilson, M., 2019. Late Oligocene–early Miocene transformation of postcollisional magmatism in Tibet. Geology 47, 776–780.

Guo, Z., Wilson, M., Zhang, M., Cheng, Z., Zhang, L., 2013. Post-collisional, K-rich mafic magmatism in south Tibet: constraints on Indian slab-to-wedge transport processes and plateau uplift. Contrib. Mineral. Petrol. 165, 1311–1340.
Guo, Z., Wilson, M., Zhang, M., Cheng, Z., Zhang, L., 2015. Post-collisional Ultrapotassic Mafic Magmatism in South Tibet: Products of Partial Melting of Pyroxenite in the Mantle Wedge Induced by Roll-back and Delamination of the Subducted Indian Continental Lithosphere Slab. J. Petrol. 56, 1365–1406.
Hermann, J., 2002. Allanite: thorium and light rare earth element carrier in subducted crust. Chem. Geol. 192, 289–306.
Hermann, J., Rubatto, D., 2009. Accessory phase control on the trace element signature of sediment melts in subduction zones. Chem. Geol. 265, 512–526.
Hill, E., Wood, B.J., Blundy, J.D., 2000. The effect of Ca-Tschermaks component on trace element partitioning between clinopyroxene and silicate melt. Lithos 53, 203–215.
Hirschmann, M.M., Kogiso, T., Baker, M.B., Stolper, E.M., 2003. Alkalic magmas generated by partial melting of garnet pyroxenite. Geology 31, 481–484.
Huang, F., Chen, J.-L., Xu, J.-F., Wang, B.-D., Li, J., 2015. Os–Nd–Sr isotopes in Miocene ultrapotassic rocks of southern Tibet: Partial melting of a pyroxenite-bearing lithospheric mantle? Geochim. Cosmochim. Acta 163, 279–298.
Huang, F., Zhang, Z., Xu, J., Li, X., Zeng, Y., Wang, B., Li, X., Xu, R., Fan, Z., Tian, Y., 2019. Fluid flux in the lithosphere beneath southern Tibet during Neo-Tethyan slab breakoff: Evidence from an appinite–granite suite. Lithos 344–345, 324–338.
Huang, F., Rooney, T.O., Xu, J.-F., Zeng, Y.-C., 2021. Magmatic record of continuous Neo-Tethyan subduction after initial India-Asia collision in the central part of southern Tibet. GSA Bull. 133, 1600–1612.
Ionov, D.A., Hofmann, A.W., 1995. Nb-Ta-Rich Mantle Amphiboles and Micas – Implications for Subduction-Related Metasomatic Trace-Element Fractionations. Earth Planet. Sci. Lett. 131, 341–356.
Kapp, P., DeCelles, P.G., 2019. Mesozoic-Cenozoic geological evolution of the Himalayan-Tibetan orogen and working tectonic hypotheses. Am. J. Sci. 319, 159–254.
Kendall, B., Dahl, T.W., Anbar, A.D., 2017. The Stable Isotope Geochemistry of Molybdenum. Rev. Mineral. Geochem. 82, 683–732.
König, S., Wille, M., Voegelin, A., Schoenberg, R., 2016. Molybdenum isotope systematics in subduction zones. Earth Planet. Sci. Lett. 447, 95–102.
Konzett, J., Armstrong, R.A., Sweeney, R.J., Compston, W., 1998. The timing of MARID metasomatism in the Kaapvaal mantle: An ion probe study of zircons from MARID xenoliths. Earth Planet. Sci. Lett. 160, 133–145.
Lee, H.Y., Chung, S.L., Lo, C.H., Ji, J.Q., Lee, T.Y., Qian, Q., Zhang, Q., 2009. Eocene Neotethyan slab breakoff in southern Tibet inferred from the Linzizong volcanic record. Tectonophysics 477, 20–35.
Leitzke, F.P., Fonseca, R.O.C., Michely, L.T., Sprung, P., Munker, C., Heuser, A., Blanchard, H., 2016. The effect of titanium on the partitioning behavior of high-field strength elements between silicates, oxides and lunar basaltic melts with applications to the origin of mare basalts. Chem. Geol. 440, 219–238.
Leitzke, F.P., Fonseca, R.O.C., Sprung, P., Mallmann, G., Lagos, M., Michely, L.T., Münker, C., 2017. Redox dependent behaviour of molybdenum during magmatic processes in the terrestrial and lunar mantle: Implications for the Mo/W of the bulk silicate Moon. Earth Planet. Sci. Lett. 474, 503–515.
Li, Y., Audétat, A., 2012. Partitioning of V, Mn Co, Ni, Cu, Zn, As, Mo, Ag, Sn, Sb, W, Au, Pb, and Bi between sulfide phases and hydrous basanite melt at upper mantle conditions. Earth Planet. Sci. Lett. 355–356, 327–340.
Li, H.-Y., Li, J., Ryan, J.G., Li, X., Zhao, R.-P., Ma, L., Xu, Y.-G., 2019. Molybdenum and boron isotope evidence for fluid-fluxed melting of intraplate upper mantle beneath the eastern North China Craton. Earth Planet. Sci. Lett. 520, 105–114.
Li, J., Liang, X.-R., Zhong, L.-F., Wang, X.-C., Ren, Z.-Y., Sun, S.-L., Zhang, Z.-F., Xu, J.-F., 2014. Measurement of the Isotopic Composition of Molybdenum in Geological Samples by MC-ICP-MS using a Novel Chromatographic Extraction Technique. Geostand. Geoanal. Res. 38, 345–354.
Li, X.H., Yan, Q.S., Zeng, Z.G., Fan, J.J., Li, S.Z., Li, J., Yang, H.X., Wang, X.Y., 2021b. Across-arc variations in Mo isotopes and implications for subducted oceanic crust in the source of back-arc basin volcanic rocks. Geology 49, 1165–1170.
Li, S.-G., Yang, W., Ke, S., Meng, X., Tian, H., Xu, L., He, Y., Huang, J., Wang, X.-C., Xia, Q., Sun, W., Yang, X., Ren, Z.-Y., Wei, H., Liu, Y., Meng, F., Yan, J., 2017. Deep carbon cycles constrained by a large-scale mantle Mg isotope anomaly in eastern China. Natl. Sci. Rev. 4, 111–120.
Li, W., Yang, Z., Massimo, C., Lai, Y., Yu, C., Zhang, J., 2020. Redox state of southern Tibetan upper mantle and ultrapotassic magmas. Geology 48, 733–736.
Li, H.-Y., Zhao, R.-P., Li, J., Tamura, Y., Spencer, C., Stern, R.J., Ryan, J.G., Xu, Y.-G., 2021a. Molybdenum isotopes unmask slab dehydration and melting beneath the Mariana arc. Nat. Commun. 12, 6015.
Liang, Y.-H., Halliday, A.N., Siebert, C., Fitton, J.G., Burton, K.W., Wang, K.-L., Harvey, J., 2017. Molybdenum isotope fractionation in the mantle. Geochim. Cosmochim. Acta 199, 91–111.
Liu, Y.S., Gao, S., Kelemen, P.B., Xu, W.L., 2008. Recycled crust controls contrasting source compositions of Mesozoic and Cenozoic basalts in the North China Craton. Geochim. Cosmochim. Acta 72, 2349–2376.
Liu, H.-Q., Li, J., Xu, Y.-G., Yumul Jr., G.P., Knittel, U., Dimalanta, C.B., Payot, B.D., Queaño, K., Huang, X.-L., Zhang, L., 2022b. Heavy Mo isotope composition of northern Bataan adakites, Philippines: Evidence for fore-arc subduction erosion? Geology.
Liu, A.-L., Wang, Q., Zhu, D.-C., Cawood, P.A., Xia, Y., Li, S.-M., Liu, S.-A., Huang, F., Liu, L., Zhao, Z.-D., Mo, X.-X., 2022a. Temporal and Spatial Variations of Enriched Source Components in Linzizong Volcanic Succession, Tibet, and Implications for the India-Asia Collision. J. Petrol. 63.
Liu, C.Z., Wu, F.Y., Chung, S.L., Zhao, Z.D., 2011. Fragments of hot and metasomatized mantle lithosphere in Middle Miocene ultrapotassic lavas, southern Tibet. Geology 39, 923–926.
Liu, D., Zhao, Z., Zhu, D.-C., Niu, Y., DePaolo, D.J., Harrison, T.M., Mo, X., Dong, G., Zhou, S., Sun, C., Zhang, Z., Liu, J., 2014. Postcollisional potassic and ultrapotassic rocks in southern Tibet: Mantle and crustal origins in response to India-Asia collision and convergence. Geochim. Cosmochim. Acta 143, 207–231.
Luguet, A., Lorand, J.P., Seyler, M., 2003. Sulfide petrology and highly siderophile element geochemistry of abyssal peridotites: A coupled study of samples from the Kane Fracture Zone (45 degrees W 23 degrees 20N, MARK Area, Atlantic Ocean). Geochim. Cosmochim. Acta 67, 1553–1570.
Ma, L., Xu, Y.-G., Li, J., Chen, L.-H., Liu, J.-Q., Li, H.-Y., Huang, X.-L., Ma, Q., Hong, L.-B., Wang, Y., 2022. Molybdenum isotopic constraints on the origin of EM1-type continental intraplate basalts. Geochim. Cosmochim. Acta 317, 255–268.
Martin, L.A.J., Hermann, J., Gauthiez-Putallaz, L., Whitney, D.L., Vitale Brovarone, A., Fornash, K.F., Evans, N.J., 2014. Lawsonite geochemistry and stability – implication for trace element and water cycles in subduction zones. J. Metam. Geol. 32, 455–478.
McCoy-West, A.J., Chowdhury, P., Burton, K.W., Sossi, P., Nowell, G.M., Fitton, J.G., Kerr, A.C., Cawood, P.A., Williams, H.M., 2019. Extensive crustal extraction in Earth's early history inferred from molybdenum isotopes. Nat. Geosci. 12, 946–951.
Mckenzie, D., Onions, R.K., 1991. Partial Melt Distributions from Inversion of Rare-Earth Element Concentrations. J. Petrol. 32, 1021–1091.
Miller, C., Schuster, R., Klötzli, U., Frank, W., Purtscheller, F., 1999. Post-Collisional Potassic and Ultrapotassic Magmatism in SW Tibet: Geochemical and Sr–Nd–Pb–O Isotopic Constraints for Mantle Source Characteristics and Petrogenesis. J. Petrol. 40, 1399–1424.
Nebel-Jacobsen, Y., Wille, M., Ivanic, T., Nebel, O., 2021. Molybdenum isotope systematics in cumulate rock of the 2.8 Windimurra layered intrusion: A test for igneous differentiation and the composition of the Archean mantle. Precambr. Res. 355, 106087.
Newsom, H.E., Palme, H., 1984. The depletion of siderophile elements in the Earth's mantle: new evidence from molybdenum and tungsten. Earth Planet. Sci. Lett. 69, 354–364.
Palme, H., O'Neill, H.S.C., 2014. 3.1 - Cosmochemical Estimates of Mantle Composition. In: Holland, H.D., Turekian, K.K. (Eds.), Treatise on Geochemistry. Second Edition. Elsevier, Oxford, pp. 1–39.
Patchett, P.J., White, W.M., Feldmann, H., Kielinczuk, S., Hofmann, A.W., 1984. Hafnium/rare earth element fractionation in the sedimentary system and crustal recycling into the Earth's mantle. Earth Planet. Sci. Lett. 69, 365–378.
Plank, T., 2005. Constraints from Thorium/Lanthanum on Sediment Recycling at Subduction Zones and the Evolution of the Continents. J. Petrol. 46, 921–944.
Prelevic, D., Akal, C., Foley, S.F., Romer, R.L., Stracke, A., Van Den Bogaard, P., 2012. Ultrapotassic Mafic Rocks as Geochemical Proxies for Post-collisional Dynamics of Orogenic Lithospheric Mantle: the Case of Southwestern Anatolia, Turkey. J. Petrol. 53, 1019–1055.
Romaniello, S.J., Herrmann, A.D., Anbar, A.D., 2016. Syndepositional diagenetic control of molybdenum isotope variations in carbonate sediments from the Bahamas. Chem. Geol. 438, 84–90.
Rudnick, R.L., Gao, S., 2014. Composition of the Continental Crust. In: Rudnick, R.L. (Ed.), Treatise on Geochemistry. Elsevier.
Salters, V.J.M., Longhi, J., 1999. Trace element partitioning during the initial stages of melting beneath mid-ocean ridges. Earth Planet. Sci. Lett. 166, 15–30.
Salters, V.J.M., Stracke, A., 2004. Composition of the depleted mantle. Geochem. Geophys. Geosyst., 5
Skora, S., Blundy, J.D., Brooker, R.A., Green, E.C.R., de Hoog, J.C.M., Connolly, J.A.D., 2015. Hydrous Phase Relations and Trace Element Partitioning Behaviour in Calcareous Sediments at Subduction-Zone Conditions. J. Petrol. 56, 953–980.
Skora, S., Freymuth, H., Blundy, J., Elliott, T., Guillong, M., 2017. An experimental study of the behaviour of cerium/molybdenum ratios during subduction: Implications for tracing the slab component in the Lesser Antilles and Mariana Arc. Geochim. Cosmochim. Acta 212, 133–155.
Sun, S., McDonough, W.F., 1989. Chemical and isotopic systematics of oceanic basalts: implications for mantle composition and processes. Geol. Soc. Lond. Spec. Publ. 42, 313–345.
Tian, S., Hou, Z., Mo, X., Tian, Y., Zhao, Y., Hou, K., Yang, Z., Hu, W., Li, X., Zhang, Y., 2020. Lithium isotopic evidence for subduction of the Indian lower crust beneath southern Tibet. Gondw. Res. 77, 168–183.
Tommasini, S., Avanzinelli, R., Conticelli, S., 2011. The Th/La and Sm/La conundrum of the Tethyan realm lamproites. Earth Planet. Sci. Lett. 301, 469–478.
Turner, S., Arnaud, N., Liu, J., Rogers, N., Hawkesworth, C., Harris, N., Kelley, S., Van Calsteren, P., Deng, W., 1996. Post-collision, shoshonitic volcanism on the Tibetan Plateau: Implications for convective thinning of the lithosphere and the source of ocean island basalts. J. Petrol. 37, 45–71.
Vervoort, J.D., Plank, T., Prytulak, J., 2011. The Hf–Nd isotopic composition of marine sediments. Geochim. Cosmochim. Acta 75, 5903–5926.
Villalobos-Orchard, J., Freymuth, H., O'Driscoll, B., Elliott, T., Williams, H., Casalini, M., Willbold, M., 2020. Molybdenum isotope ratios in Izu arc basalts: The control of subduction zone fluids on compositional variations in arc volcanic systems. Geochim. Cosmochim. Acta 288, 68–82.
Voegelin, A.R., Nägler, T.F., Pettke, T., Neubert, N., Steinmann, M., Pourret, O., Villa, I. M., 2012. The impact of igneous bedrock weathering on the Mo isotopic composition of stream waters: Natural samples and laboratory experiments. Geochim. Cosmochim. Acta 86, 150–165.

Voegelin, A.R., Pettke, T., Greber, N.D., von Niederhausern, B., Nagler, T.F., 2014. Magma differentiation fractionates Mo isotope ratios: Evidence from the Kos Plateau Tuff (Aegean Arc). Lithos 190, 440–448.
Wang, Z., Becker, H., 2018. Molybdenum partitioning behavior and content in the depleted mantle: Insights from Balmuccia and Baldissero mantle tectonites (Ivrea Zone, Italian Alps). Chem. Geol. 499, 138–150.
Wang, B., Xu, J., Zhang, X., Chen, J., Kang, Z., Dong, Y., 2008. Petrogenesis of Miocene volcanic rocks in the Sailipu area, Western Tibetan Plateau: Geochemical and Sr-Nd isotopic constraints. Acta Petrol. Sin. 24, 265–278.
Wang, B., Chen, J., Xu, J., Wang, L., 2014. Geochemical and Sr–Nd–Pb–Os isotopic compositions of Miocene ultrapotassic rocks in southern Tibet: Petrogenesis and implications for the regional tectonic history. Lithos 208–209, 237–250.
Wang, Y., Prelević, D., Foley, S.F., 2019. Geochemical characteristics of lawsonite blueschists in tectonic mélange from the Tavşanlı Zone, Turkey: Potential constraints on the origin of Mediterranean potassium-rich magmatism. Am. Mineral. 104, 724–743.
Wang, Y., Foley, S.F., Buhre, S., Soldner, J., Xu, Y., 2021. Origin of potassic postcollisional volcanic rocks in young, shallow, blueschist-rich lithosphere. Sci. Adv. 7, eabc0291.
Willbold, M., Elliott, T., 2017. Molybdenum isotope variations in magmatic rocks. Chem. Geol. 449, 253–268.
Willbold, M., Hibbert, K., Lai, Y.J., Freymuth, H., Hin, R.C., Coath, C., Vils, F., Elliott, T., 2016. High-Precision Mass-Dependent Molybdenum Isotope Variations in Magmatic Rocks Determined by Double-Spike MC-ICP-MS. Geostand. Geoanal. Res. 40, 389–403.
Wille, M., Nebel, O., Pettke, T., Vroon, P.Z., König, S., Schoenberg, R., 2018. Molybdenum isotope variations in calc-alkaline lavas from the Banda arc, Indonesia: Assessing the effect of crystal fractionation in creating isotopically heavy continental crust. Chem. Geol. 485, 1–13.
Williams, H.M., Turner, S.P., Pearce, J.A., Kelley, S.P., Harris, N.B.W., 2004. Nature of the source regions for post-collisional, potassic magmatism in southern and northern Tibet from geochemical variations and inverse trace element modelling. J. Petrol. 45, 555–607.
Xiong, X.L., Adam, J., Green, T.H., 2005. Rutile stability and rutile/melt HFSE partitioning during partial melting of hydrous basalt: Implications for TTG genesis. Chem. Geol. 218, 339–359.
Xiong, X., Keppler, H., Audétat, A., Gudfinnsson, G., Sun, W., Song, M., Xiao, W., Yuan, L., 2009. Experimental constraints on rutile saturation during partial melting of metabasalt at the amphibolite to eclogite transition, with applications to TTG genesis. Am. Mineral. 94, 1175–1186.
Yang, J., Siebert, C., Barling, J., Savage, P., Liang, Y.-H., Halliday, A.N., 2015. Absence of molybdenum isotope fractionation during magmatic differentiation at Hekla volcano, Iceland. Geochim. Cosmochim. Acta 162, 126–136.
Yang, J., Barling, J., Siebert, C., Fietzke, J., Stephens, E., Halliday, A.N., 2017. The molybdenum isotopic compositions of I-, S- and A-type granitic suites. Geochim. Cosmochim. Acta 205, 168–186.
Yin, A., Harrison, T.M., 2000. Geologic evolution of the Himalayan-Tibetan orogen. Annu. Rev. Earth Planet. Sci. 28, 211–280.
Zhang, Y., Yuan, C., Sun, M., Li, J., Long, X., Jiang, Y., Huang, Z., 2020. Molybdenum and boron isotopic evidence for carbon-recycling via carbonate dissolution in subduction zones. Geochim. Cosmochim. Acta 278, 340–352.
Zhang, Y., Huang, F., Xu, J., Zeng, Y., Wang, B., Lv, M., Zhang, L., Li, M., Zhang, Z., Tian, Y., Liu, Q., Zhang, L., 2022. Origin of the volcanic rocks in Dianzhong Formation, central Lhasa Terrane, Tibet: implication for the genesis of syn-collisional magmatism and Neo-Tethyan slab roll-back. Int. Geol. Rev.
Zhao, P.-P., Li, J., Zhang, L., Wang, Z.-B., Kong, D.-X., Ma, J.-L., Wei, G.-J., Xu, J.-F., 2016. Molybdenum Mass Fractions and Isotopic Compositions of International Geological Reference Materials. Geostand. Geoanal. Res. 40, 217–226.
Zhao, Z.D., Mo, X.X., Dilek, Y., Niu, Y.L., DePaolo, D.J., Robinson, P., Zhu, D.C., Sun, C.G., Dong, G.C., Zhou, S., Luo, Z.H., Hou, Z.Q., 2009. Geochemical and Sr-Nd-Pb-O isotopic compositions of the post-collisional ultrapotassic magmatism in SW Tibet: Petrogenesis and implications for India intra-continental subduction beneath southern Tibet. Lithos 113, 190–212.
Zhu, D.-C., Zhao, Z.-D., Niu, Y., Dilek, Y., Hou, Z.-Q., Mo, X.-X., 2013. The origin and pre-Cenozoic evolution of the Tibetan Plateau. Gondw. Res. 23, 1429–1454.
Zou, H.B., 1997. Inversion of partial melting through residual peridotites or clinopyroxenes. Geochim. Cosmochim. Acta 61, 4571–4582.